Brain-imaging evidence for compression of binary sound sequences in human memory

Samuel Planton[1]*, Fosca Al Roumi[1*+], Liping Wang[2] & Stanislas Dehaene[1,3]

[1]Cognitive Neuroimaging Unit, Université Paris-Saclay, INSERM, CEA, CNRS, NeuroSpin center, 91191 Gif/Yvette, France
[2]Institute of Neuroscience, Key Laboratory of Primate Neurobiology, CAS Center for Excellence in Brain Science and Intelligence Technology, Chinese Academy of Sciences, Shanghai 200031, China
[3]Collège de France, Université Paris Sciences Lettres (PSL), 11 Place Marcelin Berthelot, 75005 Paris, France

*Co-first authors
[+] Corresponding author
Postal address:
Cognitive Neuroimaging Unit, INSERM-CEA-University Paris Saclay NeuroSpin center, CEA/SAC/DRF/Joliot Bât 145, Point Courrier 156 F-91191 Gif/Yvette, France
E-mail: fosca.alroumi@gmail.com

Abstract

According to the language of thought hypothesis, regular sequences are compressed in human memory using recursive loops akin to a mental program that predicts future items. We tested this theory by probing memory for 16-item sequences made of two sounds. We recorded brain activity with functional MRI and magneto-encephalography (MEG) while participants listened to a hierarchy of sequences of variable complexity, whose minimal description required transition probabilities, chunking, or nested structures. Occasional deviant sounds probed the participants' knowledge of the sequence. We predicted that task difficulty and brain activity would be proportional to the complexity derived from the minimal description length in our formal language. Furthermore, activity should increase with complexity for learned sequences, and decrease with complexity for deviants. These predictions were upheld in both fMRI and MEG, indicating that sequence predictions are highly dependent on sequence structure and become weaker and delayed as complexity increases. The proposed language recruited bilateral superior temporal, precentral, anterior intraparietal and cerebellar cortices. These regions overlapped extensively with a localizer for mathematical calculation, and much less with spoken or written language processing. We propose that these areas collectively encode regular sequences as repetitions with variations and their recursive composition into nested structures.

Introduction

The ability to learn and manipulate serially ordered lists of elements, i.e. sequence processing, is central to several human activities (Lashley, 1951). This capacity is inherent to the ordered series of subtasks that make up the actions of daily life, but is especially decisive for the implementation of high-level human skills such as language, mathematics, or music. In non-human primates, multiple levels of sequence encoding ability, with increasing complexity, have been identified, from the mere representation of transition probabilities and timings to ordinal knowledge (which element comes first, second, third…), recurring chunks, and even abstract patterns (e.g. does the sequence obey the pattern xxxxY, i.e a repetition ending with a different element) (Dehaene et al., 2015; Jiang et al., 2018; Shima et al., 2007; Wang et al., 2015; Wilson et al., 2013). We and others, however, proposed that the representation of sequences in humans may be unique in its ability to encode recursively nested hierarchical structures, similar to the nested phrase structures that linguists postulate to underlie human language (Dehaene et al., 2015; Fitch & Martins, 2014; Hauser et al., 2002). Building on this idea, it was suggested that humans would spontaneously encode temporal sequences of stimuli using a language-like system of nested rules, a "language of thought" (LoT, see Fodor, 1975) (Al Roumi et al., 2021; Amalric et al., 2017; Chater & Vitányi, 2003; Feldman, 2000; Li & Vitányi, 1993; Mathy & Feldman, 2012; Planton et al., 2021; Wang et al., 2019). For instance, when faced with a sequence such as xxYYxYxY, humans may encode it using an abstract internal expression equivalent to « 2 groups of 2, and then an alternation of 4 ».

The assumption that humans encode sequences in a recursive, language-like manner, was recently tested with a non-linguistic visuo-spatial task, by asking human adults and children to memorize and track geometric sequences of locations on the vertices of an octagon (Al Roumi et al., 2021; Amalric et al., 2017; Wang et al., 2019). Behavioral and brain-imaging studies showed that such sequences are internally compressed in human memory using an abstract "language of geometry" that captures their numerical and geometrical regularities (e.g., "next element clockwise", "vertical symmetry"). Indeed, behavioral results showed that the difficulty of memorizing a sequence was linearly modulated, not by the actual sequence length, but by the length of the program capable of generating it using the proposed language ("minimal description length" or MDL; for a definition and brief review, see Dehaene et al., 2022). The length of this program provides a predictor of sequence complexity. We will,

from now on, refer to it as LoT-complexity. In a follow-up fMRI experiment where participants had to follow the same sequences with their gaze, activity in the dorsal part of inferior prefrontal cortex correlated with the LoT-complexity while the right dorsolateral prefrontal cortex (dlPFC) encoded the presence of embedded structure (Wang et al., 2019). These results indicate that sequences are stored in memory in a compressed manner, the size of this code being the length of the shortest program that describes the sequence in the proposed formal language. Memory for sequences would therefore follow the "minimal description length" principle inherited from information theory (Grunwald, 2004) and often used to capture various human behaviors (Chater & Vitányi, 2003; Feldman, 2000; Mathy & Feldman, 2012). Wang et al. (2019) further showed that the encoding and compression of such sequences involved brain areas supporting the processing of mathematical expressions rather than language-related areas, suggesting that multiple internal languages, not necessarily involving classical language areas, are present in the human brain. In a follow-up study, Al Roumi et al. (2021) showed with MEG that the spatial, ordinal, and geometrical primitive codes postulated in the proposed LoT could be extracted from brain activity.

In the present work, we ask whether this LoT may also explain the human memory for binary auditory sequences (i.e. sequences made up of only two possible items, for instance two sounds with high and low pitch, respectively). While arguably minimal, binary sequences preserve the possibility of forming structures at different hierarchical levels. They therefore provide an elementary window into the mental representation of nested language-like rules, and which aspect of this representation, if any, is unique to the human species. While it would make little sense to ask if non-human animals can store spoken human sentences, it does seem more reasonable to submit them to a protocol with minimal, binary sound sequences, and ask whether they use a recursive language-like format for encoding in memory, or whether they are confined to statistical learning or chunking. The latter mechanisms are important to consider because they are thought to underpin the processing of several aspects of sequence processing in human infants and adults as well as several animal species, such as the extraction of chunks within a stream of syllables, tones or shapes (Wang et al., 2019), or the community structure that generates a sequence of events (Karuza et al., 2019; Schapiro et al., 2013). Yet, very few studies have tried to separate the brain mechanisms underlying rule-based predictions from those of probabilistic sequence learning (Bhanji et al., 2010; Kóbor et al., 2018; Maheu et al., 2021). Our goal here is to develop such a paradigm in humans,

and to test the hypothesis that human internal models are based on a recursive language of thought.

The present work capitalized on a series of behavioral experiments (Planton et al., 2021) in which we proved that human performance in memorizing binary auditory sequences, as tested by the capacity to detect occasional violations, could be predicted by a modified version of the language of geometry, based on the hierarchical combination of very few primitives (repeat, alternate, concatenate, and integers). This work considered binary sequences of various lengths (from 6 to 16 items) mainly in the auditory but also in the visual modality, and showed that LoT-complexity was correlated with participants' oddball detection performance. This was especially true for longer sequences of 16 items as their length exceeds typical working memory capacity (Cowan, 2001, 2010; Miller, 1956) and therefore requires compression. In this work, LoT predictions were compared to competitor models of cognitive complexity and information compression (Aksentijevic & Gibson, 2012; Alexander & Carey, 1968; Delahaye & Zenil, 2012; Gauvrit et al., 2014; Glanzer & Clark, 1963; Psotka, 1975; Vitz & Todd, 1969). The predictive power of LoT outperformed all competing theories (Planton et al., 2021).

Here, we use functional MRI and magneto-encephalography to investigate the cerebral underpinnings of the proposed language in the human brain. We exposed participants to 16-item auditory binary sequences, with varying levels of regularity, while recording their brain activity with fMRI and MEG in two separate experiments (see Figure 1). By combining these two techniques, we aimed at obtaining both the spatial and the temporal resolution needed to characterize in depth the neural mechanisms supporting sequence encoding and compression.

In both fMRI and MEG, the experiment was composed of two phases. In a habituation phase, the sequences were repeatedly presented in order for participants to memorize them, thus probing the complexity of their internal model. In a test phase, sequences were occasionally presented with deviants (a single tone A replacing another tone B), thus probing the violations of expectations generated by the internal model (Figure 1B). We focused on a very simple prediction arising from the hierarchical predictive coding framework (Friston, 2005). According to this view, and to much experimental research (e.g. Bekinschtein et al., 2009; Chao et al., 2018; Heilbron & Chait, 2018; Summerfield & de Lange, 2014; Wacongne et al., 2011), the internal model of the sequence, as described by the postulated LoT, would be

encoded by prefrontal regions of the brain, which would send anticipation signals to auditory areas, where they would be subtracted from incoming signals. As a consequence, we predict a reciprocal effect of LoT on the brain signals during habituation and during deviancy. In the habituation part of the experiment, lower amplitude response signals should be observed for sequences of low complexity – and conversely, during low complexity sequences, we expect top-down predictions to be stronger and therefore deviants to elicit larger responses, than for complex, hard to predict sequences.

Two subtleties further qualify this overall theoretical picture. First, at the highest level of sequence complexity, sequences cannot be compressed in a simple LoT expression, and therefore we expect the brain areas involved in nested sequence coding to exhibit no further increase in activation, or even a decrease (Vogel & Machizawa, 2004; Wang et al., 2019). We will evaluate the presence of such a non-linear trend by testing a quadratic term for LoT-complexity in addition to a purely linear term in the regression models. Second, a simpler system of statistical learning, based on transition probabilities, may operate in parallel with LoT predictions (Bekinschtein et al., 2009; Chao et al., 2018; Maheu et al., 2019, 2021; Meyniel et al., 2016; Summerfield & de Lange, 2014). To separate their contributions, we will use multiple predictors in a general linear model of behavior and of MEG signals, whose temporal resolution allows to track individual sequence items (in fMRI, the BOLD response was too slow relative to the sequence rate of 250 ms per item).

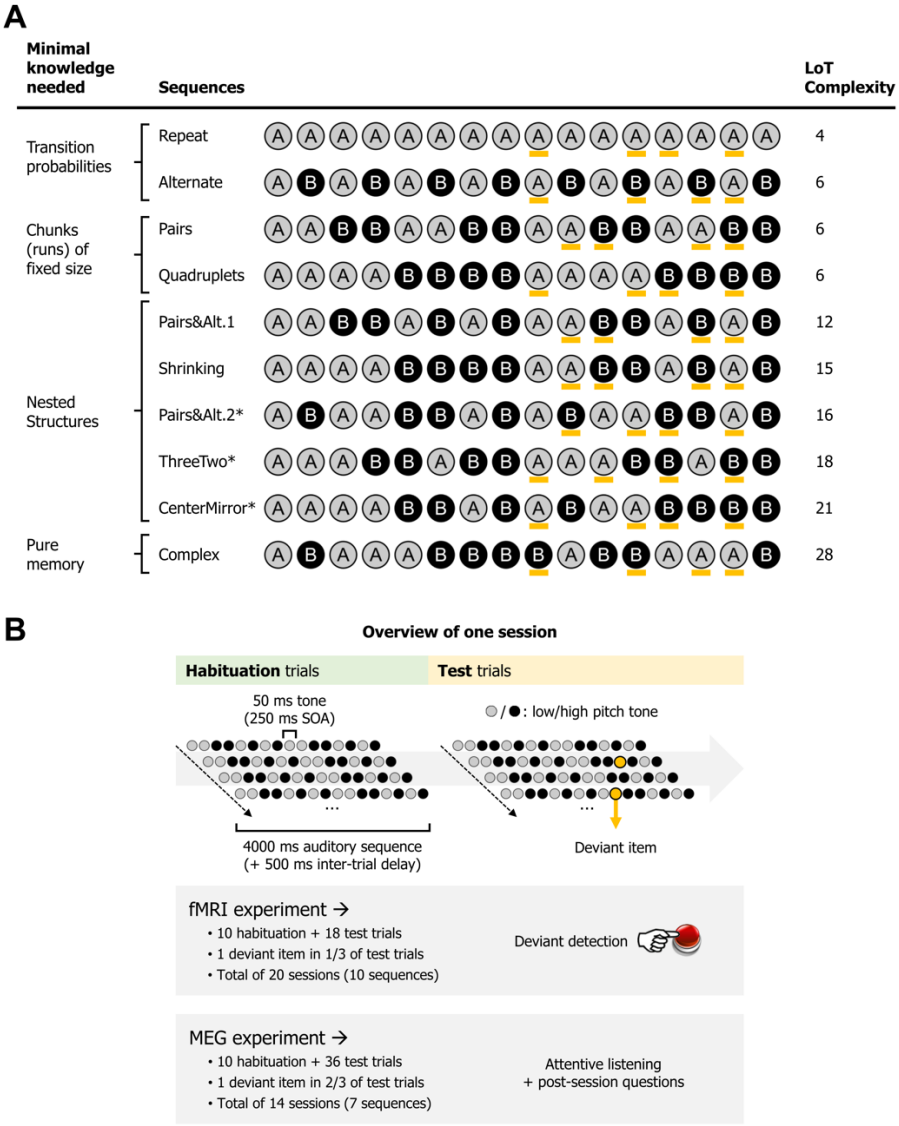

Figure 1. Experimental design. A) List of the different 16-items sequences used in the MEG and fMRI experiments, with associated LoT complexity, and categorized according to the type of knowledge assumed to be required for optimal memory encoding. Orange marks indicate positions in which violations could occur (4 possible positions per sequence, all between positions 9 and 15). *Sequences used only in the fMRI experiment. Sequence description provided by the LoT and the corresponding verbal description. This verbal description is meant ease the understanding of the formal expression. B) Overview of the presentation paradigm (example with a session the Pairs&Alt.1 sequence), with the respective characteristics of the fMRI experiment and the MEG experiment. One unique sequence was used in any given session. Each sequence was tested twice, in two different sessions (reversing the mapping between A/B items and low/high pitch).

Results

The Language of Thought for binary sequences

As used in the present work, the Language of Thought (LoT) hypothesis postulates that humans encode mental objects such as sequences or geometric shapes using “mental programs”, i.e expressions in a symbolic language characterized by (1) a small set of primitives (2) the capacity to recursively combine these primitives through three operators: concatenation, repetition (possibly with variations), and recursive nesting (i.e. calling of a subprogram) (Dehaene et al., 2022; Sablé-Meyer et al., 2022). In this framework, defining a language requires the selection of a vocabulary of primitives that be recursively combined.

The language for binary sequences that we evaluate here is an adaptation of a LoT for spatial sequences with geometrical regularities, which accounted for participants’ predictions in an explicit sequence completion task (Amalric et al., 2017) and in a gaze anticipation task (Wang et al., 2019). Previous fMRI and MEG studies have found neural evidence that human participants use such a LoT to encode geometrical sequences in memory and predict upcoming items (Al Roumi et al., 2021; Wang et al., 2019). For an in-depth description of this language, please see supporting information in Amalric et al. (2017).

In Planton et al., 2021, we showed how the very same language could also account for the compression of auditory sequences made of two sounds. To obtain this language for binary sequences, instead of the eight vertices of the octagon, we consider only two states, A and B (e.g. a high-pitch and a low-pitch tone). The primitive operations are now reduced to the *stay* operation (called *+0*) and the *change* operation (called *b*). Note that, similarly to a Turing machine, the descriptions are sequential: each operation is relative to the previous state. The repetition operation, denoted by ^n, allows any sequence of operations to be repeated *n* times, possibly with variations, denoted by <>. For instance the instruction "[xxx]^2<+0>" indicates that the expression [xxx] is executed twice, with the same starting point: "<+0>", while "[xxx]^2<b>" indicates that the expression [xxx] is executed twice, with a change in the starting point: "<b>" (see Figure S1).

The description length of a mental program is computed as a weighted sum of the fixed costs attached to each primitive instruction (see supporting information in Amalric et al., 2017). The cost for repeating an instruction *n* times is assumed to correspond to log10(n) (rounded up), i.e. the number of digits needed to encode the number in decimal notation. Note that any given sequence has several possible descriptions. For instance, AAAA could be described as [+0,+0,+0,+0] or in a more compact manner as [+0]^4. LoT-complexity is the minimal description length of a sequence, i.e. the shortest possible description of it in the proposed language.

In our previous work, we compared extensively the proposed LoT to other sequence encoding models such as entropy, change complexity or algorithmic complexity (Planton et al., 2021). The findings indicated that LoT complexity for chunk-preserving expressions, i.e. those that do not split any chunk of repetitions, provided the best fit of participants' behavior, over and above all other competing models. The present study builds on these results and investigates the neural code of the LoT.

Stimulus design

We designed a hierarchy of sequences (figure 1) of fixed length (16 items) that should systematically vary in complexity according to our previously proposed language of thought (Planton et al., 2021) and whose gradations separate the lower-level representations of sequences that may be accessible to non-human primates (as outlined in Dehaene et al., 2015) from the more abstract ones that may only be accessible to humans (Figure 1A).

Figure 1 presents the sequences we selected for the experiments, their complexity and a short verbal description of their minimal program (in Figure S1, we also give the formal (LoT) description). The sequences formed a hierarchy. At the lowest level, much evidence indicates that the brain spontaneously encodes statistical regularities such as transition probabilities in sequential sensory inputs and uses them to make predictions (e.g. Barascud et al., 2016; Bendixen et al., 2009; McDermott et al., 2013; Meyniel et al., 2016; Saffran et al., 1996), an ability well within the grasp of various non-human animals (e.g Hauser et al., 2001; Meyer & Olson, 2011). The first two sequences in our hierarchy therefore consisted in predictable repetitions (AAAA…) and alternations (ABABA…). In terms of information compression, such

199 sequences can be represented with a very short LoT expression (a mere repetition, or a
200 repetition of alternations).

201 At the next level, we tested chunking, the ability to group a recurring set of contiguous
202 items into a single unit, another major sequence encoding mechanism which is also accessible
203 to non-human primates (Buiatti et al., 2009; Fujii & Graybiel, 2003; Saffran et al., 1996; Sakai
204 et al., 2003; Uhrig et al., 2014). Thus, we included sequences made of pairs (AABBAABB…) or
205 quadruplets (AAAABBBB…). Our LoT model attributes them a high level of compressibility, but
206 already some degree of hierarchy (a loop of chunks). Relative to the previous sequences, they
207 require monitoring the number of repetitions before a new chunk starts (ABABA… = 1;
208 AABBAA… = 2; AAAABBBB… = 4), and may therefore be expected to engage the number
209 system, though to involve the bilateral intraparietal sulci, particularly their horizontal and
210 anterior segments (Dehaene et al., 2003; Eger et al., 2009; Harvey et al., 2013; Kanayet et al.,
211 2018).

212 The next level required nested structures, i.e. a hierarchical representation of smaller
213 chunks embedded in larger chunks. Although there is some debate on whether this level of
214 representation can be accessed by non-human animals, especially with extensive training
215 (Ferrigno et al., 2020; Gentner et al., 2006; Jiang et al., 2018; van Heijningen et al., 2009), many
216 agree that the ability to access it quickly and spontaneously is a potential human-specific trait
217 in sequence learning and many related cognitive domains (Dehaene et al., 2015; Fitch, 2004;
218 Fitch & Martins, 2014; Hauser et al., 2002). We probe it using a variety of complex but
219 compressible sequences such as "AABBABABAABBABAB" (whose hierarchical description is
220 $[A^2B^2[AB]^2]^2$ and can be paraphrased as "a repetition of two pairs followed by four
221 alternations). Here again, our LoT model easily compresses such nested structures by using
222 only one additional bit whenever a chunk needs to be repeated, regardless of its hierarchical
223 depth (for details, see Amalric et al., 2017).

224 Finally, as a control, our paradigm also includes a high-complexity, largely
225 incompressible sequence, with balanced transition probabilities and minimal chunking
226 possibilities. We selected a sequence which our language predicted to be of maximal
227 complexity (highest MDL), and which was therefore predicted to challenge the limits of
228 working memory (Figure 1A). Note that because such a complex sequence, devoid of recurring
229 regularities, is not easily encodable within our language (except for a trivial concatenation of

chunks), we expect the brain areas involved in nested sequence coding to exhibit no further increase in activation, or even a decrease (Vogel & Machizawa, 2004).

Behavior in deviant detection

Similar to Planton et al. (2021), we used task performance in the fMRI deviant detection task to quantify the LoT model's ability to predict behavior. Sensitivity (d') was calculated by examining the hit rate for each sequence and each violation position, relative to the overall false-alarm rate on standard no-violation trials. On average, participants managed to detect the deviants at above chance level in all sequences and at all positions (min d'= 0.556, min $t(22) = 2.919$, $p < .0080$). Thus, they were able to detect a great variety of violation types in regular sequences (unexpected alternations, repetitions, change in number, or chunk boundaries). However, performance worsened as the 16-item sequences became too complex to be easily memorized. The group-averaged performance in violation detection for each sequence (regardless of deviant position) was linearly correlated with LoT complexity, both for response times to correctly detected items (RTs) ($F(1, 8) = 43.87$, $p < .0002$, $R^2 = .85$) and for sensitivity (d') ($F(1, 8) = 159.4$, $p < .0001$, $R^2 = .95$) (see Figure 2A). When including the participants as a random factor in a linear mixed model, we obtained a very similar result for sensitivity ($F(1, 206) = 192.92$, $p < .0001$, with estimates of -0.092 ± 0.007 for the LoT complexity predictor, and 3.39 ± 0.17 for the intercept), as well as for responses times ($F(1, 203) = 110.87$, $p < .0001$, with estimates of 17.4 ms ± 1.6 for the LoT complexity predictor, and 475.4 ms ± 38.6 for the intercept). As for false alarms, they were rare, and no significant linear relationship with LoT complexity was found in group averages ($F(1, 8) = 2.18$, $p = .18$), although a small effect was found in a linear mixed model with participant as the random factor ($F(1, 206) = 4.83$, $p < .03$, with estimates of 0.038 ± 0.017 for the LoT complexity predictor, and 1.57 ± 0.39 for the intercept).

We evaluated whether these results could be explained by statistical learning, i.e. whether deviants were more easily or more rapidly detected when they violated the transition probabilities of the current sequence. For sensitivity (d'), a likelihood ratio test showed that adding a transition-probability measure of surprise (Maheu et al., 2019; Meyniel et al., 2016) to the linear regression with LoT complexity improved the goodness of fit ($\chi^2(1) = 4.35$, $p < .038$). The effect of transition-based surprise was indeed significant in the new model (F(1,

205) = 4.35, $p < .039$), but LoT complexity effect remained highly significant ($F(1, 205) = 106.28$, $p < .0001$). Similarly, for RTs, adding transition-based surprise to the model significantly improved model fit ($\chi^2(1) = 12.27$, $p < .0005$). Transition-based surprise explained some of the variance in RTs ($F(1, 202) = 12.51$, $p < .0006$), but again the effect of LoT complexity remained highly significant ($F(1, 202) = 46.3$, $p < .0001$).

We also added a quadratic complexity term to the models to determine whether the trend was purely linear (i.e., performance degrading continuously with complexity) or also had a non-linear component (e.g., "plateau" performance after reaching a certain level of complexity). For sensitivity, a quadratic term did not improve goodness of fit, whether transition-based surprise was also included ($\chi^2(1) = 1.58$, $p = .21$) or not ($\chi^2(1) = 0.02$, $p = .89$). For RTs, it did not improve goodness of fit in the model including transition-based surprise ($\chi^2(1) = 1.43$, $p = .23$), but it did when transition-based surprise was not included ($\chi^2(1) = 6.76$, $p < .010$). These results indicates that the effect of complexity on behavior is primarily linear, although a non-linear trend may be present on response times, as suggested by examining figure 2A.

We then assessed whether alternative models of sequence complexity could better explain the present behavioral data, in an analysis similar to Planton et al. (2021). The five alternative accounts we considered were: *Entropy*, a measure of information that quantifies the uncertainty of a distribution, here based on transition pairs (Maheu et al., 2021); *Lempel-Ziv complexity*, derived from the popular lossless data compression algorithm (Lempel & Ziv, 1976); *Number of Subsymmetries*, proposed by Alexander & Carey (1968), which is the number of symmetric sub-sequences of any length within a sequence; *Chunk Complexity*, a measure of the number of runs or chunks weighted by their length (Mathy & Feldman, 2012; Planton et al., 2021); and *Change complexity*, a metric proposed by Aksentijevic & Gibson (2012), quantifying the average amount of "change" across all sub-sequences contained in a sequence (see Planton et al., 2021 for additional details on these metrics). As before, for each of these metrics plus LoT, we fitted two linear mixed models, with and without the transition-based surprise regressor, resulting in twelve models for sensitivity and twelve models for RTs. All models included participants as a random factor along with the fixed factor(s). The Akaike information criterion (AIC) was used as an indicator of goodness of fit. As presented in Figure 2B, for sensitivity, the best models to predict performance were, in this order, "LoT complexity + Surprise" (AIC = 582.9, conditional $R^2 = 0.62$), "LoT complexity" (AIC = 587.9, conditional R^2

= 0.62) and "Change complexity + Surprise" (AIC = 610.8, conditional R^2 = 0.55). For RTs, the best models were "LoT complexity + Surprise" (AIC = 3031.2, conditional R^2 = 0.55), "Change complexity + Surprise" (AIC = 3038.1, conditional R^2 = 0.52) and "Change complexity" (AIC = 610.8, conditional R^2 = 0.52). Regardless of the complexity metric, adding the transition-based surprise regressor in the model always resulted in improved goodness of fit (reduction in AIC of 18.54 on average for sensitivity, and 18.49 for RTs).

In summary, using a partially different set of sequences, we replicated the behavioral findings of Planton et al. (2021): for long sequences that largely exceed the storage capacity in working memory, violation detection and response speed (both indexing the ease of memorizing the sequence and anticipating the next item) were well correlated with the LoT model of sequence compression, which outperformed other approaches for quantifying sequence complexity.

Behavioral bracketing task

After brain imaging, we also asked all participants to report their intuitions of how each sequence should be parsed by drawing brackets on a visual representation of its contents (after listening to it). The results (see heatmaps in Figure 2C) indicated that participants agreed about how a sequence should be parsed and used bracketing levels appropriately for nested sequences. For instance, they consistently placed brackets in the middle of sequences that consisted in two repetitions of 8 items, but did so less frequently both within those phrases and when the midpoint was not a predicted parsing point (CenterMirror in figure 2C). In order to assess the correspondence between the parsings and the organization proposed by the LoT model, we computed for each sequence the correlation between the group-averaged number-of-brackets vector and the LoT model vector (obtained from the sequence segmentation derived from the LoT description in terms of repeat, alternate and concatenate instructions). A strong correlation was found for sequences *Repeat* (Pearson r = 0.96, p < .0001), *Pairs* (r = 0.88, p < .0001), *Quadruplets* (r = 0.96, p < .0001), *Pairs&Alt.1* (r = 0.94, p < .0001), *Shrinking* (r = 0.93, p < .0001), *Pairs&Alt.2* (r = 0.85, p < .0001), *ThreeTwo* (r = 0.95, p < .0001), *CenterMirror* (r = 0.95, p < .0001) and *Complex* (r = 0.84, p < .0001), but not for *Alternate* (r = 0.08, p = .77). For the latter, a departure from the proposed encoding was found: while the shortest LoT representation encodes it as "15 alternations", the participants' parses

corresponded to “8 AB pairs”. In the discussion, we explain how this small departure from theory could have arisen from the specifics of the visual bracketing task, rather than the actual encoding of the auditory sequence.

It could be suggested that, rather than the structure predicted by the LoT model, participants use transition probabilities to segment a sequence, with rare transitions acting as chunk boundaries. We thus tested the correlations between the group-averaged number-of-brackets vector and the transition-based surprise derived from transition probabilities. There are 15 item-to-item transitions in 16-item sequences, thus brackets before the first and after the last items were excluded from this analysis. Surprise was computed by pooling over all the transitions in a given sequence. Due to lack of variance, a correlation with transition-based surprise was impossible for sequences *Repeat* (all transitions are 100% predictable repetitions) and *Alternate* (all transitions are 100% predictable alternations). For other sequences, a positive correlation was found for sequences *Quadruplets* ($r = 0.99$, $p < .0001$), *Pairs* ($r = 0.88$, $p < .0001$), *Complex* ($r = 0.79$, $p < .0005$), *Shrinking* ($r = 0.73$, $p < .002$), *ThreeTwo* ($r = 0.68$, $p < .006$), and *CenterMirror* ($r = 0.64$, $p < .02$). Crucially, however, no positive correlation was found for sequences *Pairs&Alt.1* ($r = -0.48$, $p = .071$) and *Pairs&Alt.2* ($r = -0.58$, $p < .03$). This was due to the fact, in these sequences, that repetitions were the rarest and therefore the most surprising transitions: thus in these sequences, transition probabilities predicted a breaking of the chunks of repeated item, while participants correctly did not do so and placed their brackets at chunk boundaries (Planton et al., 2021). Thus, although surprise arising from the learning of transition probabilities can partially predict participants’ bracketing behavior in some cases, notably when a sequence is composed of frequent repetitions and rare alternations, this model completely fails in other (e.g., when repetitions are rare), again indicating that higher-level models such as LoT are needed to explain behavior.

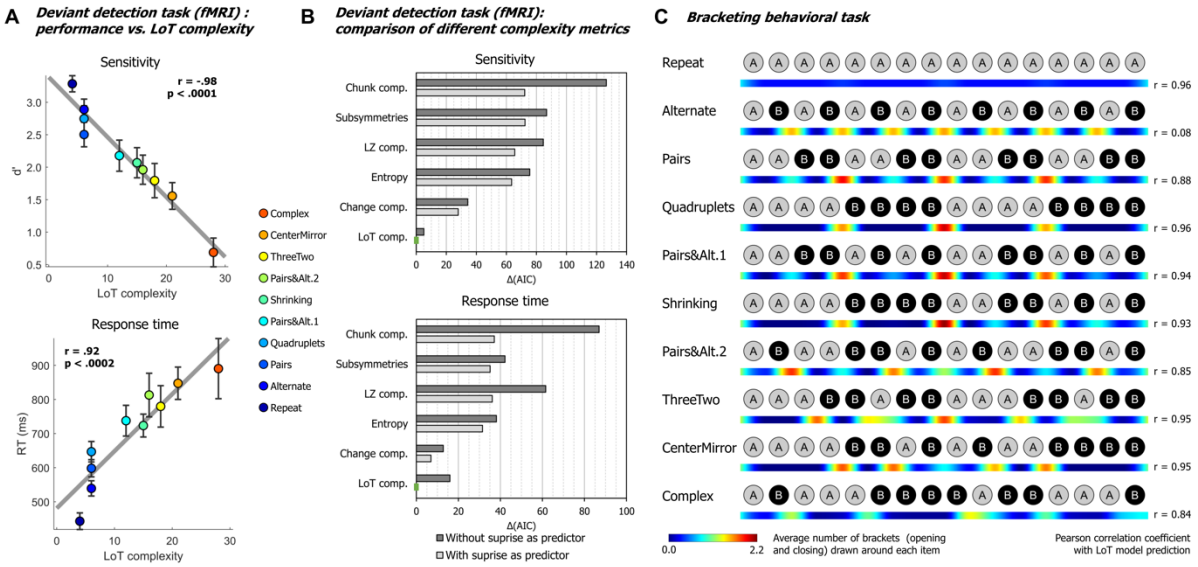

Figure 2. Behavioral data. A) Group-averaged sensitivity (*d'*) and response times for each sequence in the deviant detection task, plotted against the LoT complexity. A significant linear relationship with LoT complexity was found in both cases. The Pearson correlation coefficient and associated p-value are reported. Error bars represent SEM. **B)** Comparison of the goodness of fit (indexed by the Akaike Information Criterion) of twelve mixed models (for sensitivity, top, and for response time, bottom), i.e., each testing one out of 6 different complexity metrics (see main text) and including or not a transition-based surprise predictor. *Δ(AIC)* is the difference in AIC with the best model of the twelve. A lower value indicates a better fit. The best model (Δ(AIC) = 0) is marked by a green rectangle on the vertical axis. **C)** The heatmap for each sequence represent the vector of the average number of brackets draw by the participants around each item in the sequence bracketing task (after smoothing for illustration purposes). The Pearson correlation coefficient with the vector of brackets predicted by the LoT model is reported on the right side. A high correlation was obtained for all sequences but *Alternate*, since several subjects segmented this sequence in 8 groups of 2 items, while the shortest LoT expression represented it in a single group of 16 items with 15 alternations.

In summary, using a partially different set of sequences, we replicated the behavioral findings of Planton et al. (2021) showing that, especially for long sequences that largely exceed the storage capacity in working memory, violation detection (an index of learning quality) and response speed (potentially indexing the degree of predictability) were well predicted by our language-of-thought model of sequence compression.

fMRI data

A positive effect of complexity during sequence learning and tracking

As predicted, during the habituation phase (i.e. during sequence learning), fMRI activation mostly increased with sequence complexity in a broad and bilateral network involving supplementary motor area (SMA), precentral gyrus (preCG) abutting the dorsal part of Brodmann area 44, cerebellum (lobules VI and VIII), superior and middle temporal gyri (STG/MTG), and the anterior intraparietal sulcus region (IPS, close to its junction with the

postcentral gyrus) (Figure 3A and Table 1). These regions partially overlapped with those observed in sequence learning for a completely different domain, yet a similar language: the visuo-spatial sequences of Wang et al. (2019). In the opposite direction, a reduction of activation with complexity was seen in a smaller network, mostly corresponding to the default-mode network, which was increasingly deactivated as working memory load increased (Mazoyer et al., 2001; Raichle, 2015): medial frontal cortex, left middle cingulate gyrus, left angular gyrus (AG) and left pars orbitalis of the inferior frontal gyrus (IFGorb) (Table 1).

We then computed the same contrast with the standard trials of the test phase (sequences without violation). The network of areas showing a positive complexity effect was much smaller than during habituation: it included bilateral superior parietal cortex extending into the precuneus, left dorsal premotor area as well as two cerebellar regions (right lobule IV, left lobule VIII) (Figure S2, Table S1). These areas were also found during the habituation phase, although the (predominantly left) parietal superior / precuneus activation was larger and extended more posteriorily than during habituation. Regions showing a negative LoT complexity effect in standard trials (reduced activation for increasing complexity) were more numerous: medial frontal regions, middle cingulate gyri, bilateral angular gyrus, bilateral anterior part of the inferior temporal gyrus, bilateral putamen, as well as left frontal orbital region and left occipital gyrus. Here again, they largely resemble what was already observed in habituation trials (i.e. a deactivation of a default mode network), with a few additional elements such as the putamen.

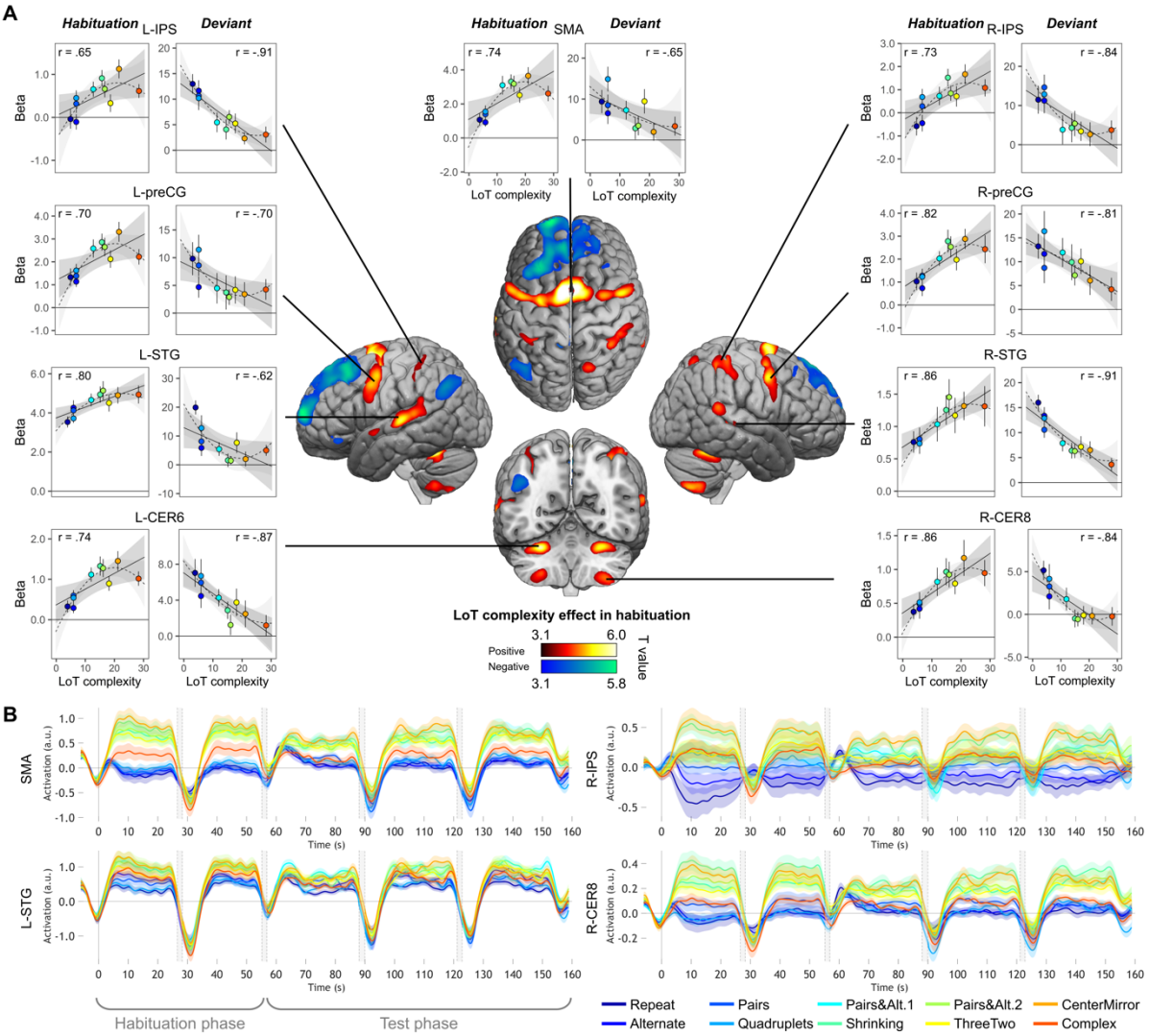

Figure 3. Sequence complexity in the proposed language of thought (LoT) modulates fMRI responses to standard and deviant sequences. **A)** brain areas showing an increase (hot colors) or a decrease (cold colors) in activation with sequence LoT complexity during habituation (voxel-wise $p < .001$, uncorrected; cluster-wise $p < .05$, FDR corrected). Scatterplots represent the group-average activation for each of the ten sequences as a function of their LoT complexity (left panels: habituation trials; right panels, deviant trials) in each of nine ROIs. Data values are from a participant-specific ROI analysis. Error bars represent SEM. Linear trend are represented by a solid line (with 95% CI in dark grey) and quadratic trend by a dashed line (with 95% CI in light grey). Pearson linear correlation coefficients are also reported. **B)** Time course of group-averaged BOLD signals for each sequence, for four representative ROIs. Each mini-session lasted 160-seconds and consisted of 28 trials divided into 5 blocks (2 × 5 habituation and 3 × 6 test trials), interspersed with short rest periods of variable duration (depicted in light gray). The full time course was reconstituted by resynchronizing the data at the onset of each successive block (see Methods). Shading around each time course represents one SEM.

406 **Table 1. Coordinates of brain areas modulated by LoT complexity during habituation**

Positive LoT complexity effect in habituation trials

Region	H	k	p(unc.)	p(FWE-corr)	T	x	y	z
Supplementary motor area, Precentral gyrus, Superior frontal gyrus (dorsolateral), Middle frontal gyrus	L/R	8991	<.0001	<.0001	6.62	-1	5	65
			<.0001	<0.001	5.82	-8	12	49
			<.0001	<.05	5.59	-27	-5	52
Lobule VIII of cerebellar hemisphere	L	1411	<.0001	<.0001	6.19	22	-68	-53
Lobule VI and Crus I of cerebellar hemisphere	L	939	<.0001	<0.001	5.97	-29	-56	-28
Superior temporal gyrus, Middle temporal gyrus	L	2022	<.0001	<.05	5.56	-68	-23	5
			<.0001	<.05	4.80	-59	-35	12
			<.0001	0.213	4.25	-55	-42	23
Lobule VI of cerebellar hemisphere	R	1216	<.0001	<.05	5.45	27	-58	-27
Lobule VIII of cerebellar hemisphere	L	1549	<.0001	<.05	5.04	-22	-67	-53
			<.0001	0.118	4.44	-33	-54	-55
Superior temporal gyrus	R	1039	<.0001	<.05	4.93	48	-30	3
			<.0001	<.05	4.79	67	-44	17
			<0.001	0.880	3.55	69	-23	3
Postcentral gyrus, Inferior parietal gyrus	R	1478	<.0001	<.05	4.79	36	-46	56
			<.0001	0.061	4.63	46	-35	61
			<.0001	0.170	4.33	46	-32	47
Superior parietal gyrus, Precuneus	R	547	<.0001	0.085	4.54	17	-67	58
			<0.001	0.792	3.65	24	-60	42
Inferior parietal gyrus, Postcentral gyrus	L	1570	<.0001	0.106	4.47	-31	-42	44
			<.0001	0.149	4.37	-45	-35	38
			<.0001	0.530	3.90	-40	-42	61

Negative LoT complexity effect in habituation trials

Region	H	k	p(unc.)	p(FWE-corr)	T	x	y	z
Superior frontal gyrus (dorsolateral, medial, medial orbital), Middle frontal gyrus	L/R	12366	<.0001	<0.001	5.86	-19	67	12
			<.0001	<.05	5.42	-29	25	47
			<.0001	<.05	5.33	-6	44	58
Middle cingulate & paracingulate gyri, Precuneus	L	1444	<.0001	<.05	5.26	-1	-33	51
Angular gyrus	L	1530	<.0001	0.060	4.63	-43	-65	37
			<0.001	0.816	3.63	-33	-54	24
			<0.001	0.938	3.45	-27	-82	44
IFG pars orbitalis	L	522	<.0001	0.354	4.07	-52	35	-14
			<.0001	0.473	3.95	-34	40	-7
			<.0001	0.645	3.80	-27	33	-16

407

408 ## A negative effect of complexity on deviant responses

409 The effect of LoT complexity at the whole brain level was first assessed on the responses to all
410 deviant stimuli (whether detected or not). A positive linear effect of complexity was only
411 found in a small cluster of the medial part of the superior frontal gyrus (SFG) (Table S2). As
412 predicted, a much larger network showed a negative effect (i.e. reduced activation with
413 complexity or increased activation for less complex sequences): bilateral postcentral gyrus
414 (with major peak in the ventral part), supramarginal gyrus (SMG), IPS, STG, posterior MTG,

415 ventral preCG, Insula, SMA and middle cingulate gyrus, cerebellum (lobules VI, VIII, and
416 vermis), right pars triangularis of the IFG (red activation map of Figure 4, Table S2). This
417 network is thus the possible brain counterpart of the increase in deviant detection
418 performance observed as sequences become less and less complex. However, this result could
419 be partly due to a motor effect, since manual motor responses to deviants were less frequent
420 for more complex sequences, as attested by an effect of LoT complexity on sensitivity. We
421 therefore computed the same contrast using an alternative GLM modeling only deviant trials
422 to which the participant correctly responded (note that this model consequently included
423 fewer trials, especially for higher complexity sequences). Negative effects of LoT complexity
424 were still present in this alternative model, now unconfounded by motor responses. As shown
425 in Figure 4 (yellow) the negative effect network was a subpart of the network identified in the
426 previous model, and concerned bilateral STG, MTG, SMG/postcentral gyrus, Insula, SMA and
427 middle cingulate gyrus. A positive effect was still present in a medial SFG cluster, part of the
428 default-mode network showing less deactivation for deviants as complexity increased.

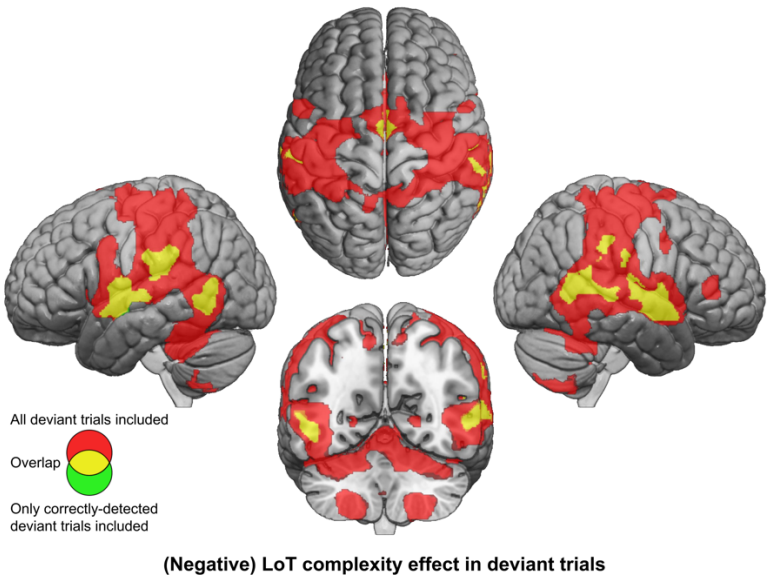

429
430 **Figure 4. Brain responses to deviants decrease with LoT complexity.** Colors indicate the brain areas whose
431 activation on deviant trials decreased significantly with complexity, in two distinct general linear models (GLMs):
432 one in which all deviant stimuli were modeled (red), and one in which only correctly-detected deviant stimuli
433 were modeled (green) (voxel-wise $p < .001$, uncorrected; cluster-wise $p < .05$, FDR corrected). Overlap is shown
434 in yellow.

435 **ROI analyses of the shape of the complexity effect**

436 We next used individual ROIs to measure the precise shape of the complexity effect
437 and test the hypothesis that (1) activation increases with complexity but may reach a plateau
438 or decrease for the most complex, incompressible sequence; and (2) on deviant trials, the

complexity effect occurs in the opposite direction. Because merely plotting the signal at peaks identify by a linear or quadratic contrast would bias the results (Vul et al., 2009), we designed cross-validated individual ROI analyses, which consisted in (1) using half of the runs to identify responsive subject-specific voxels within each ROI, using a contrast of positive effect of complexity during habituation; and (2) using the other half to extract the activation levels for each standard or deviant sequence (only the initial search volumes were still defined on the basis of the entire data from the present study, which is likely to introduce only a minimal degree of circularity). We focused on nine areas that exhibited a positive complexity contrast in habituation (figure 3), where the effect was robust and was computed on the learning phase of the experiment, therefore uncontaminated by deviant stimuli and manual motor responses.

In each ROI, mixed effect models with participants as the random factor were used to assess the replicability of the linear effect of complexity during habituation. A significant effect was found in all ROIs (after Bonferroni correction for nine ROIs), although with variable effect size: SMA: β estimate = 0.10, $t(21) = 5.37$, p.corr < .0003; L-STG: $\beta = 0.06$, $t(21) = 4.75$, p.corr < .001; L-CER6: $\beta = 0.04$, $t(21) = 4.73$, p.corr < .002; R-IPS: $\beta = 0.07$, $t(21) = 4.08$, p.corr < .005; L-preCG: $\beta = 0.07$, $t(21) = 3.98$, p.corr < .007; R-preCG: $\beta = 0.08$, $t(21) = 3.8$, p.corr < .01; R-STG: $\beta = 0.03$, $t(21) = 3.35$, p.corr < .03; R-CER8: $\beta = 0.03$, $t(21) = 3.32$, p.corr < .03 and L-IPS: $\beta = 0.03$, $t(21) = 3.25$, p.corr < .04. These results are illustrated in Figure 3A, showing the linear regression trend with values averaged per condition across participants. The addition of a quadratic term was significant for seven ROIs (SMA, L-CER6, L-IPS, L-preCG, L-STG, R-CER8 and R-IPS), but did not reached significance in R-preCG nor in R-STG. This effect was always negative, indicating that the activation increases with complexity reached saturation or decreased from the most complex sequence (see dashed lines in the scatter plots of Figure 3A).

We also examined the time course of activation profiles within each mini-session of the experiment, i.e. two habituation blocks followed by three test blocks. As shown in Figure 3B (see Figure S3 for all 9 ROIS), the activation time courses showed a brief activation to sequences, presumably corresponding to a brief search period. 5 to 10 seconds following the first block onset, however, activation quickly dropped to a similar and very low activation, or even a deactivation below the rest level, selectively for the 4 lowest-complexity sequences which involved only simple processes of transition probabilities or chunking. For other

sequences, the BOLD effect shot up in rough proportion to complexity, yet with a midlevel amplitude for the most complex sequence reflecting the saturation, quadratic effect noted earlier. Thus, in 5-10 seconds, the profile of the complexity effect was firmly established, and it remained sustained over time during habituation and, with reduced amplitude, during test blocks. This finding indicated that the same areas were responsible for discovering the sequence profile and for monitoring it for violations during the test period. The profile was similar across regions, with one exception: while most areas showed the same, low activation to the first four, simplest sequences, the left and right IPS showed an increasing activation as a function of the number of items in a chunk (ABABAB… = 1; AABBAA… = 2; AAAABBBB… = 4). This observation fits with the hypothesis that these regions are involved in numerosity representation, and may therefore implement the repetitions postulated in our language.

The ROI analyses were next performed with data from the deviant trials, in order to test whether areas previously identified as sensitive to sequence complexity when learning the sequence also showed an opposite modulation of their response to deviant trials. All ROIs indeed showed a significant negative effect of LoT complexity: R-STG: $\beta = -0.46$, $t(197) = -8.01$, $p.corr < .0001$; L-IPS: $\beta = -0.44$, $t(197) = -6.35$, $p.corr < .0001$; R-CER8: $\beta = -0.23$, $t(197) = -5.09$, $p.corr < .0001$; L-STG: $\beta = -0.45$, $t(197) = -4.61$, $p.corr < .0001$; L-CER6: $\beta = -0.23$, $t(197) = -4.57$, $p.corr < .0001$; R-preCG: $\beta = -0.37$, $t(197) = -3.92$, $p.corr < .002$; R-IPS: $\beta = -0.49$, $t(197) = -3.85$, $p.corr < .002$; SMA: $\beta = -0.33$, $t(197) = -3.57$, $p.corr < .004$ and L-preCG: $\beta = -0.27$, $t(197) = -2.9$, $p.corr < .04$. Interestingly, unlike during habituation, the addition of a quadratic term did not improve the regression except in a single area, L-STG: $\beta = 0.05$, $t(196) = 3.9$, $p.corr < .002$. Smaller effects of the quadratic term were present in three other areas, but they were not significant after Bonferonni correction: R-CER8: $\beta = 0.02$, $t(196) = 2.68$, $p < .009$; R-STG: $\beta = 0.02$, $t(196) = 2.42$, $p < .02$ and L-IPS: $\beta = 0.02$, $t(196) = 2.3$, $p < .03$.

As in the whole-brain analysis, we finally conducted a complementary analysis using activation computed with correctly-detected deviants trials only. The linear LoT complexity was now only significant in four of the nine ROIs: R-STG: $\beta = -0.48$, $t(197) = -7.64$, $p.corr < .0001$; L-IPS: $\beta = -0.34$, $t(197) = -4.54$, $p.corr < .0001$; L-STG: $\beta = -0.42$, $t(197) = -4.12$, $p.corr < .0006$; R-CER8: $\beta = -0.15$, $t(197) = -3.17$, $p.corr < .02$. When adding a quadratic term, no significant effects were observed at the predefined threshold, although uncorrected ones were present for L-STG: $\beta = 0.03$, $t(196) = 2.37$, $p < .02$ and R-CER8: $\beta = 0.01$, $t(196) = 2.05$, $p < .05$.

503 **Overlap with the brain networks for language and mathematics**

504 Past and present behavioral results suggest that an inner "language" is required to
505 explain human memory for auditory sequences – but is this language similar to natural
506 language, or to the language of mathematics, and more specifically geometry, from which it
507 is derived (Al Roumi et al., 2021; Amalric et al., 2017; Wang et al., 2019) ? By including in our
508 fMRI protocol an independent language and mathematics localizer experiment, we tested
509 whether the very same cortical sites are involved in natural sentence processing,
510 mathematical processing, and auditory sequences.

511 At the whole-brain group level, large amount of overlap was found between the
512 mathematics network (whole-brain mental computation > sentences processing contrast, in a
513 2nd level ANOVA analysis of the localizer experiment) and the LoT complexity network (see
514 Figure 5A): SMA, bilateral precentral cortex, bilateral anterior IPS, and bilateral cerebellum
515 (lobules VI). Some overlap was also present, to a lower extent, with the language network
516 (auditory and visual sentences > auditory and visual control stimuli) and the LoT complexity
517 network: left STG, SMA, left precentral gyrus, and right cerebellum.

518 Such group-level overlap, however, could be misleading since they involve a significant
519 degree of intersubject smoothing and averaging. For a more precise assessment of overlap,
520 we extracted, for each subject and within each of 7 language-related and 7 math-related ROIs
521 (see figure 5), the subject-specific voxels that responded, respectively, to sentence processing
522 and to mental calculation (same contrasts as above, but now within each subject). We then
523 extracted the results from those ROIs and examined their variation with LoT complexity in the
524 main experiment (during habituation). In the language network, a significant positive effect of
525 LoT complexity during the habituation phase was only found in left IFGoper: $\beta = 0.03$, $t(197) =$
526 4.25, p.corr < .0005 (Figure 5B). In fact, most other language areas showed either no activation
527 or were deactivated (e.g. IFGorb, aSTS, TP, TPJ). As concerns deviants, a significant negative
528 effect of LoT complexity was found in left IFGoper: $\beta = -0.23$, $t(197) = -3.04$, p.corr < .04; and
529 in left pSTS: $\beta = -0.24$, $t(197) = -3.27$, p.corr < .02. The quadratic term was never found
530 significant.

531 On the contrary, in the mathematics-related network, all areas showed a positive LoT
532 complexity effect in habituation (Figure 5B): SMA: $\beta = 0.05$, $t(197) = 5.6$, p.corr < .0001; left
533 preCG/IFG: $\beta = 0.05$, $t(197) = 5.03$, p.corr < .0001; right IPS: $\beta = 0.05$, $t(197) = 4.69$, p.corr <
534 .0001; right preCG/IFG: $\beta = 0.05$, $t(197) = 4.56$, p.corr < .0002; right SFG: $\beta = 0.04$, $t(197) = 4$,

p.corr < .002; left IPS: β = 0.04, t(197) = 3.78, p.corr < .003 and left SFG: β = 0.02, t(197) = 3.15, p.corr < .03. The quadratic term in the second model was also significant for three of them: SMA: β = -0.01, t(196) = -4.11, p.corr < .0009; right preCG/IFG: β = 0, t(196) = -3.21, p.corr < .03 and left preCG/IFG: β = 0, t(196) = -3.1, p.corr < .04. A negative complexity effect for deviant trials reached significance in four areas: left IPS: β = -0.42, t(197) = -4.44, p.corr < .0003; left preCG/IFG: β = -0.48, t(197) = -4.31, p.corr < .0004; right IPS: β = -0.41, t(197) = -4, p.corr < .002 and SMA: β = -0.29, t(197) = -2.97, p.corr < .05. Their response pattern was not significantly quadratic.

To summarize, all dorsal regions previously identified as involved in mathematical processing regions were sensitive to the complexity of our auditory binary sequences, as manifested by an increase, up to a certain level of complexity, during habituation; and, for most regions, a reduction of the novelty to deviants (especially for SMA, left preCG and IPS). Such a sensitivity to complexity was conspicuously absent from language areas, except for the left pars opercularis of the IFG.

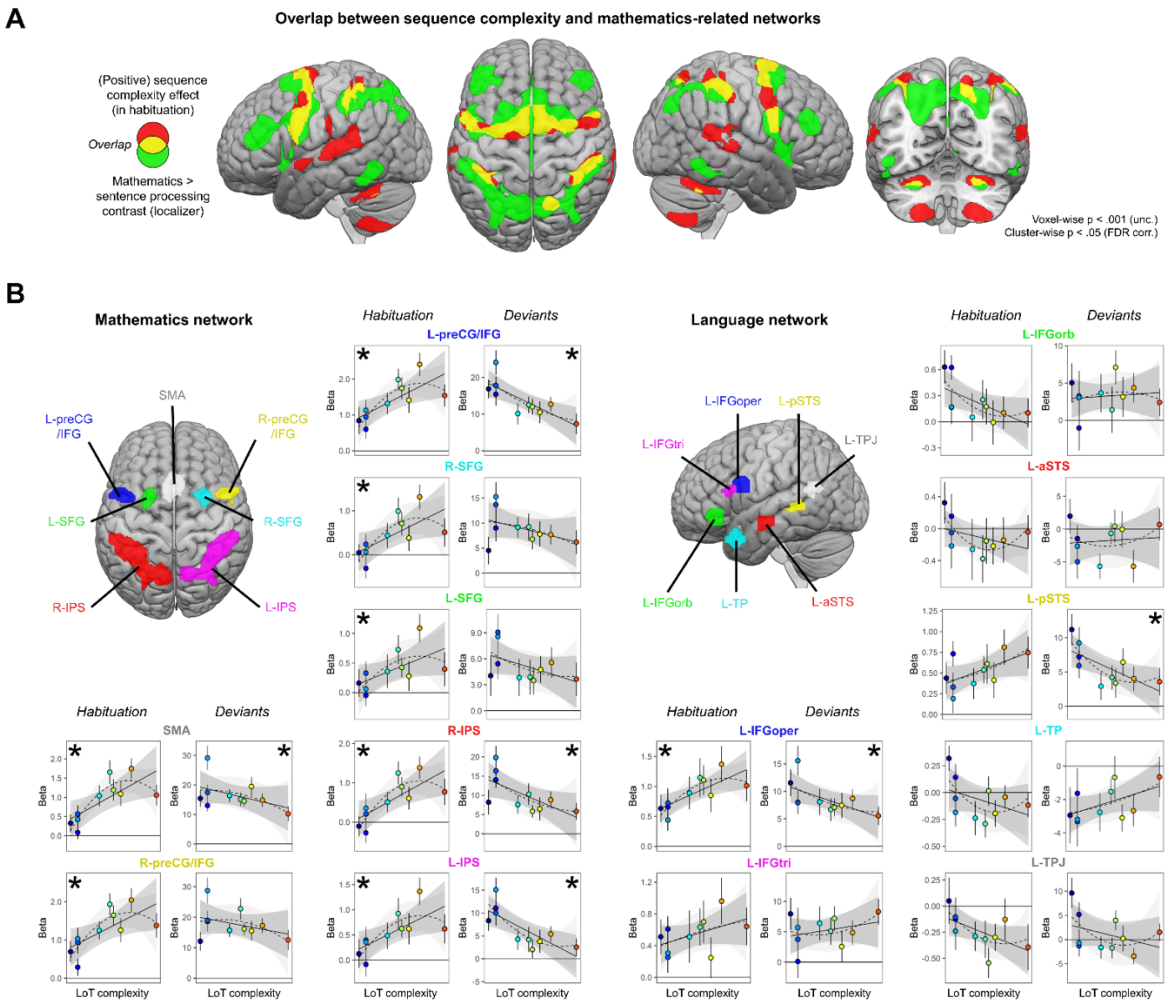

Figure 5. Sequence complexity effects in mathematics and language networks. A) Overlap between the brain areas showing an increase of activation with sequence LoT complexity during habituation in the main experiment (in red) and the brain areas showing an increased activation for mathematical processing (relative to simple listening/reading of non-mathematical sentences) in the localizer experiment (in green; both maps thresholded at voxel-wise $p < .001$ uncorrected, cluster-wise $p < .05$, FDR corrected). Overlap between the two activation maps is shown in yellow. **B)** Overview of the 7 search volumes representing the mathematics network (left) and the 7 search volumes representing the language network (right) used in the ROI analyses. Within each ROI, each scatter plot represents the group-average activation for each of the ten sequences according to their LoT complexity, for habitation blocks and for deviant trials (same format as figure 3). A star (*) indicates significance of the linear effect of LoT complexity in a linear mixed-effects model.

MEG Results

The low temporal resolution of fMRI did not permit us to track the brain response to each of the 16 successive sequence items, nor to any local sequence properties such as item-by-item variations in surprise. To address this limit, a similar paradigm was tested with MEG. To maximize signal-to-noise, especially on rare deviant trials, only seven sequences were selected (figures 1 and 6). Unlike the fMRI experiment, during MEG we merely asked participants to listen carefully to the presented sequences of sounds, without providing any button response, thus yielding pure measures of violation detection uncontaminated by the need to respond.

Neural signatures of complexity at the univariate level

We first determine if a summary measure of brain activity, the Global Field Power, is modulated by sequence complexity. To do so, we consider the brain responses to sounds occurring in the *habituation* phase, to non-deviant sounds occurring in the test phase (referred to as *standard* sounds) and to *deviant* sounds. On *habituation* trials, the late part of the auditory response (108ms – 208ms) correlated positively with complexity ($p = 0.00024$, see shaded area in the top panel of Figure 6A): the more complex the sequence, the larger the brain response. On *standard* trials, this modulation of the GFP by complexity had vanished (middle panel of Figure 6A). Finally, as predicted, the GFP computed on the *deviant* exhibited the reversed effect, i.e. a negative correlation with complexity on the 116 - 300 ms time-window ($p = 0.0005$) and on the 312 – 560 ms time-window ($p = 0.0005$), indicating that *deviants* elicit larger brain responses in sequences with lower complexity (bottom panel of Figure 6A).

To better characterize the mechanisms of sequence coding, we ran a linear regression of the evoked responses to sounds as a function of sequence complexity. Regression coefficients of

the sequence complexity predictor were projected to source space. The results showed that complexity effects were present in temporal and precentral of the cortex. To assess the significance of the regression coefficients, we ran a spatiotemporal cluster-based permutation test at the sensor level. Several significant clusters were found for each of the 3 trial types (*habituation :* cluster 1 from 72 to 216 ms, p = 0.0004, cluster 2 from 96 to 212 ms, p = 0.0002; *standard* : cluster 1 from 96 to 180ms, p = 0.0038, cluster 2 from 96 to 184 ms, p = 0.001; *deviant* : cluster 1 from 60 to 600 ms, p = 0.0002, cluster 2 from 56 to 600 ms, p = 0.0002). Figure 6 illustrates one significant cluster for each trial type. See Figure S7 for all the clusters.

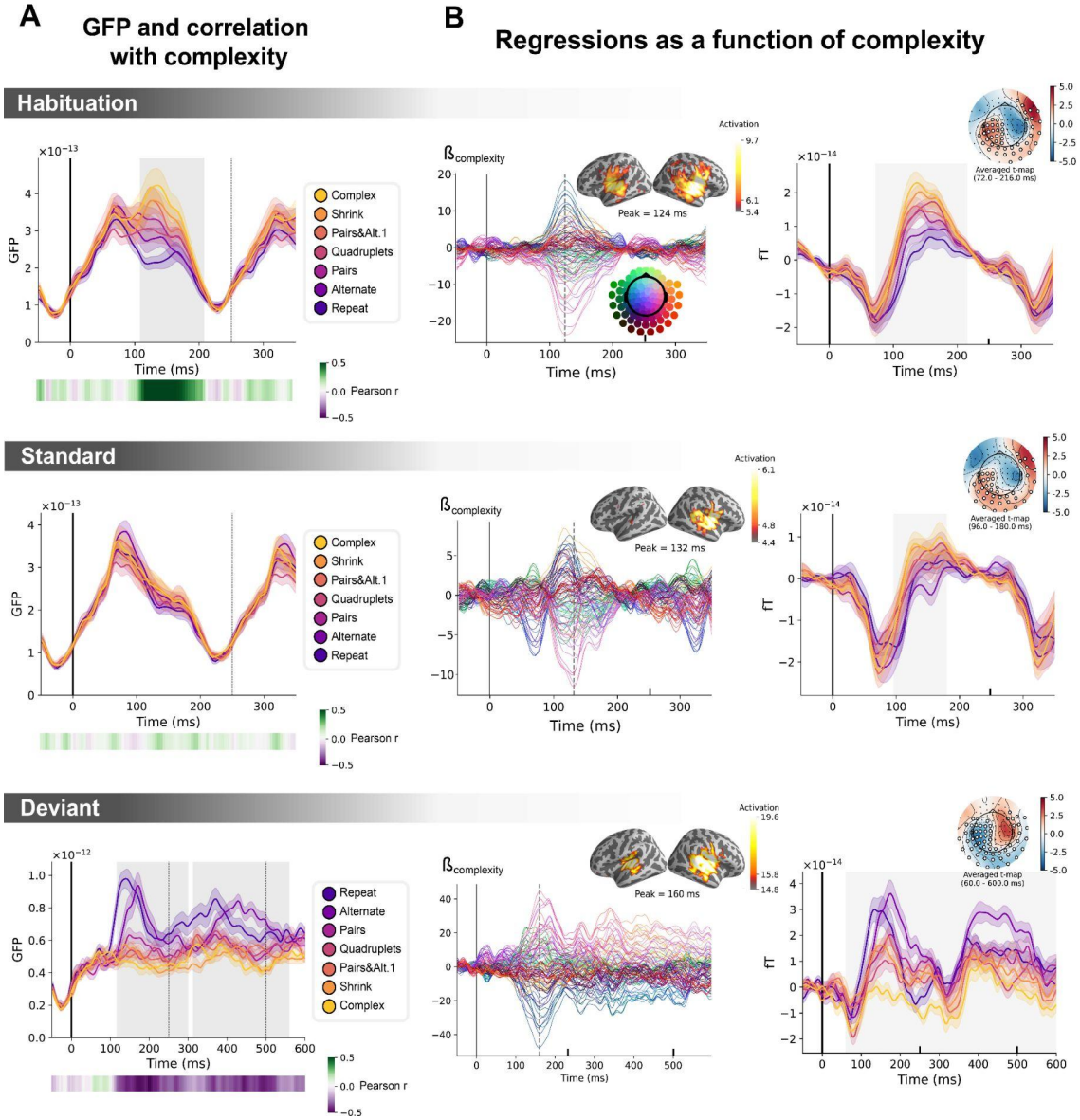

Figure 6. Sequence complexity in the proposed language of thought (LoT) modulates MEG signals to habituation, standard and deviant trials. A) Global field power computed for each sequence (see color legend) from the evoked potentials of the *Habituation, Standard* and *Deviant* trials. 0 ms indicates sound onset. Note that the time-window ranges until 350 ms for *Habituation* and *Standard* trials (with a new sound onset at S0A=250 ms), and until 600 ms for *Deviant* trials and for the others. Significant correlation with sequence complexity was found in *Habituation* and *Deviant* GFPs and are indicated by the shaded areas. **B)** Regressions of

MEG signals as a function of sequence complexity. Left: amplitude of the regression coefficients ß of the complexity regressor for each MEG sensor. Insets show the projection of those coefficients in source space at the maximal amplitude peak, indicated by a vertical dotted line. Right: spatiotemporal clusters where regression coefficients were significantly different from 0. While several clusters were found (see Text and Figure S7), for the sake of illustration, only one is shown for each trial type. The clusters involved the same sensors but on different time windows (indicated by the shaded areas) and with an opposite T-value for *Deviant* trials. Neural signals were averaged over significant sensors for each sequence type and were plotted separately.

The same analyses were performed on the contrast of Deviants – Matched Standards conditions. Matched-Standard trials are selected such that they matched the deviants' ordinal position, which was specific to each sequence. These results are reported in Figure S5. The clusters shown involve the same sensors but exhibit opposite regression signs for the brain responses to *Deviant* sounds, suggesting that, as in fMRI, the same brain regions are involved in the processing of standard and deviant items but are affected by complexity in an opposite manner.

Controlling for local transition probabilities

Several studies have shown that human EEG/MEG responses are sensitive to the statistics of sounds and sound transitions in a sequence (Maheu et al., 2019; Meyniel et al., 2016; Näätänen et al., 1989; Todorovic et al., 2011; Todorovic & Lange, 2012; Wacongne et al., 2012), including in infants (Saffran et al., 1996). When listening to probabilistic binary sequences of sounds, early brain responses reflect simple statistics such as item frequency while later brain responses reflect more complex, longer-term inferences (Maheu et al., 2019). Since local transition-based surprise and global complexity were partially correlated in our sequences, could this surprise alone account for our results? To disentangle the contributions of transition probabilities and sequence structure in the present brain responses, we regressed the brain signals as a function of complexity and of surprise based on transition probabilities. To capture the latter, we added several predictors: the presence of a repetition or an alternation and the surprise of an ideal observer that makes optimal inferences about transition probabilities from the past 100 items (see Maheu et al., 2019 for details). Both predictors were computed for two consecutive items: the one at stimulus onset (t=0ms) and the next item (t=250ms later) and included together with LoT complexity as multiple regressors of every time point.

Figure S6 shows the temporal profile of the regression coefficient for sequence complexity for each MEG sensor and its projection onto the source space, once these controlling variables were introduced. The contribution of auditory regions was slightly

634 diminished compared to the simple regression of brain signals as a function of complexity. To
635 assess the significance of the regression coefficient, we ran a spatiotemporal cluster-based
636 permutation test at the sensor level. Several significant clusters were found for each of the 3
637 trial types (*habituation :* cluster 1 from 96 to 244 ms, p = 0.0162, cluster 2 from 112 to 220 ms,
638 p = 0.014 ; *standard* : cluster 1 from 104.0 to 180.0 ms, cluster-value= 1.50, p = 0.0226, cluster
639 2 from 100 to 220 ms, p = 0.0004; *deviant* : cluster 1 from 224 to 600 ms, p = 0.0088, cluster
640 2 from 116 to 600 ms, p = 0.0006; see Figures S6 and S7 for complete cluster profiles). The
641 results remained even when the transition-based surprise regressors were entered first, and
642 then the regression on complexity was performed on the residuals (figure S6, right column).
643 In summary, the positive effect of complexity on habituation and standard trials, and its
644 negative effect on deviant trials, were not solely due to local transition-based surprise signals.

645 **Time-resolved decoding of violation responses**

646 The above results were obtained by averaging sensor data across successive stimuli
647 and across participants. A potentially more sensitive analysis method is multivariate decoding
648 is a manner similar to King & Dehaene, 2014, which searches, at each time point and within
649 each participant, for an optimal pattern of sensor activity reflecting a given type of mental
650 representation. Therefore, to further characterize the brain representations of sequence
651 structure and complexity, we next used multivariate time-resolved analyses, which allowed us
652 to track sequence coding for each item in the sequence, at the millisecond scale.

653 We trained a decoder to classify all standard versus all deviant trials (El Karoui et al.,
654 2015; King et al., 2013). As the two versions of the same sequence were presented on two
655 separated runs (respectively starting with sound 'x' or 'Y'), we trained and tested the decoder
656 in a leave-one-run out manner, thus forcing it to identify non-stimulus specific sequence
657 violation responses. In addition, and most importantly, we selected standard trials that
658 matched the deviants' ordinal position, which was specific to each sequence (see figure 1,
659 orange lines). Figure 7 shows the average projection on the decision vector of the classifier's
660 predictions on left-out data for the different sequences, when tested on both position-
661 matched *Deviants* versus *Standards* (Figure 7A) and on *Habituation* trials (Figure 7B).
662 Significance was determined by temporal cluster-based permutation tests.

663 Decoding of deviants reached significance for all sequences except for the most
664 complex ones (*Shrinking* and *Complex*). For the simplest *Repeat* and *Alternate* sequences,

which could be learned solely based on transition probabilities, a sharp initial mismatch response was seen, peaking at ~150 ms. For all other sequences, the decoder exhibited a later, slower, lower-amplitude and sustained development of above-chance performance, suggesting that deviant items elicit decodable long-lasting brain signals. A temporal cluster-based permutation test on Pearson correlation with sequence complexity showed that the decoding of violations significantly correlated with complexity (temporal cluster from 90 to 580 ms).

The time courses of the decoder performance on habituation trials also revealed a clear hierarchy in the time it took for the brain to decide that a given tone was not a deviant (figure 7B). The seven curves were ordered by predicted sequence complexity. Thus, the decoder's classification as Standard, quantified as the projection on the decision vector, decreased significantly with sequence complexity over two time windows (temporal cluster from ~90 to 220 ms and ~330 to 460 ms). This suggests that the more the sequence is complex, the more brittle its classification as Standard is.

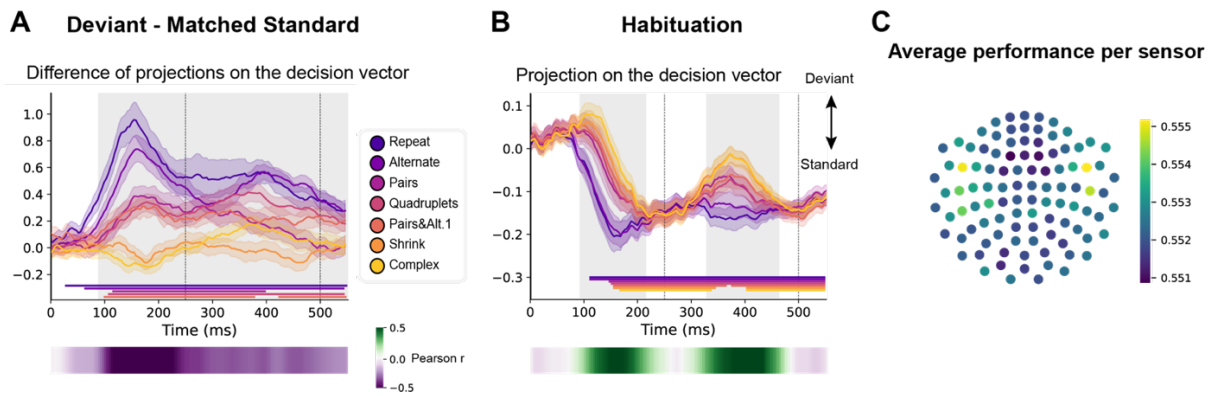

Figure 7. Multivariate decoding of deviant trials from MEG signals, and its variation with sequence complexity. A, A decoder was trained to classify standard from deviant trials from MEG signals at a given time point. We here show the difference in the projection on the decision vector for *Standard* and *Deviant* trials, that is a measure of the decoder's accuracy. The decoder was trained jointly on all sequences, but its performance is plotted here for left-out trials separately for each sequence type. Shaded areas indicate s.e.m. and colored lines at bottom indicate the time windows identified by the temporal cluster-based permutation test ($p<0.05$ corrected) obtained from cluster-based permutation test on the full window. The heatmap at the bottom represents the correlation of the performance with sequence complexity (Pearson's r). The gray shaded time-window in the main graph indicates the time-window identified by the two tailed $p<0.05$, temporal cluster-based permutation test. **B,** Projection on the decision vector for *Habituation* trials. The early brain response is classified as deviant but later as standard. This projection time-course is increasingly delayed as a function of sequence complexity (same format as **A**). **C,** sensor map showing the relative contribution of each sensor to overall decoding performance. At the time of maximal overall decoding performance (165 ms) we trained and tested 4000 new decoders that used only a subset of 40 gradiometers at 20 sensor locations. For each sensor location, the color on the maps in the right column indicates the average decoding performance when this sensor location was used in decoding, thus assessing its contribution to overall decoding.

Decoder performance over the full extent of each sequence

To characterize the time course of brain activity over the entire course of each sequence, we projected each MEG time point onto the decoding axis of the standard/deviant decoder trained on data from a 130-210 ms time window (Figure 8). The projection was computed separately for each sequence, separately for habituation, standard, and the four possible positions of deviant trials. We determined if deviants differed from standards using a cluster-based permutation test on a 0 - 600ms window after each violation (colored lines at the bottom of each sequence in Figure 8A).

All individual deviants elicited a decodable response (see *Materials and Methods*) except for the two highest-complexity sequences: *Shrinking* and *Complex* (failure at all positions exception the last one, i.e. 15). Interestingly, for the alternate sequence, two consecutive peaks indicate that, when a single repetition is introduced in an alternating sequence (e.g. ABAB**B**BAB… instead of ABABABAB…), the brain interprets it as two consecutive violations, probably due to transition probabilities, as each of the B items is predicted to be followed by an A.

Most crucially, the analysis of specific violation responses allowed us to evaluate the range of properties that humans use to encode sequences, and to test the hypothesis that they integrate numerical and structural information at multiple nested levels (Wang et al., 2015). First, within a chunk of consecutive items, they detect violations consisting in both chunk shortening (1 repeated tone instead of 2 in *Pairs*; 3 tones instead of 4 in *Quadruplets*) and chunk lengthening (3 repeated tones instead of 2, as well as 5 instead of 4). The contrast between those two sequences clearly shows that participants possess a sophisticated context-dependent representation of each sequence. Thus, their brain emits a violation response upon hearing 3 consecutive items (AA**A**) within the *Pairs* sequence, where it is unexpected, but not when the same sequence occurs within the *Quadruplets* sequence. Conversely, participants are surprised to hear the transition BBAA**B** in the *Quadruplet* context, but not in the *Pairs* context. Finally, in the *Pairs+Alt.1* sequence, such context dependence changes over time, thus indicating an additional level of nesting: at positions 9-12, subjects expect to hear two pairs (AABB) and are surprised to hear A**B**BB (unexpected alternation), but just a second later, at positions 13-16, they expect an alternation (ABAB) and are surprised to hear A**A**AB (unexpected repetition). Similar, though less significant, evidence for syntax-based violation

727 responses is present in the *Shrinking* sequence, which also ends with two pairs and an
728 alternation.

729 Figure 8 also shows in detail how the participants' brain fluctuates between
730 predictability (in blue) and violation detection (in red) during all phases of the experiment.
731 Initially, during habituation (top line), sequences are partially unpredictable, as shown by red
732 responses to successive stimuli, but that effect is strongly modulated by complexity, as
733 previously reported (red responses, particularly for the most complex sequences). In a sense,
734 while the sequence is being learned, all items in those sequences appear as deviants. As
735 expected, after habituation, the deviancy response to standards is much reduced, but still
736 ordered by complexity. Higher-complexity sequences such as *Shrinking* thus create a globally
737 less predictable environment (red colors) relative to which the violation responses to deviants
738 appear to be reduced.

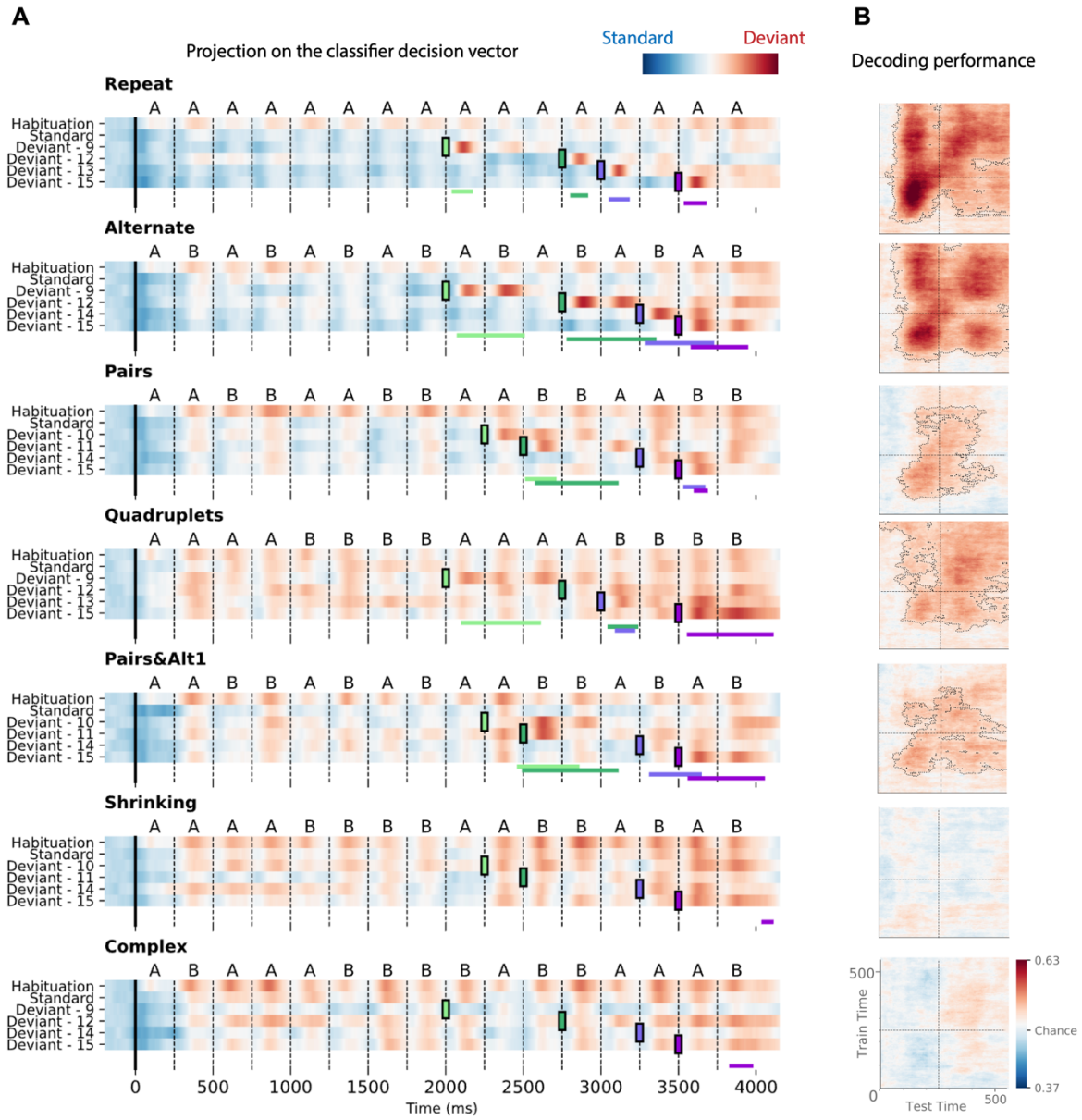

Figure 8. Time course of the deviancy decoder across the different types of sequences and deviant positions. A) Average projection of MEG signals onto the decoding axis of the standard/deviant decoder. For each sequence, the time course of the projection was computed separately for habituation trials, standard trials, and for the four types of trials containing a deviant at a given position. The figure shows the average output of decoders trained between 130 ms and 210 ms post-deviant. Red indicates that a trial tends to be classified as a deviant, blue as a standard. Colored lines at the bottom of each graph indicate the time windows obtained from the cluster permutation test comparing deviants and standards in a 0-600 ms window after deviant onset. **B**) Average generalization-across-time (GAT) matrices showing decoding performance as a function of decoder training time (y axis) and testing time (x axis). Vertical and horizontal lines indicate the onset of the next tone. The dashed lines outline $p < 0.05$ cluster-level significance, corrected for multiple comparisons (see Methods). Simpler sequences exhibit overall greater and more sustained performance. We note that, while deviancy detection does not reach significance for Shrinking and Complex sequences in the GAT matrices, violation signals reached significance for deviant position 15.

Figure 8B also shows how the Standard-Deviant decoder generalizes over time, separately for each sequence. The performance for the *Repeat* sequence exhibits a peak

corresponding to the deviant item's presentation (~ 150 ms) and a large and a partial square pattern, indicating a sustained maintenance of the deviance information. The performance for the *Alternate* sequence shows 4 peaks spaced by the SOA, corresponding to the two deviant transitions elicited by the deviant item. *Pairs, Quadruplets* and *Pairs+Alt.1* sequences still show significant decoding but not *Shrinking* and *Complex* sequences, indicating that the ability to decode deviant signals decreases with complexity.

Discussion

The goal of this study was to characterize the mental representation that humans utilize to encode binary sequences of sounds in memory and to detect occasional deviants. The results indicate that, in the human brain, deviant responses go way beyond the sole detection of violations in habitual sounds (May & Tiitinen, 2010) or in transition probabilities (Wacongne et al., 2012), and are also sensitive to more complex, larger-scale regularities (Bekinschtein et al., 2009; Bendixen et al., 2007; Maheu et al., 2019; Schröger et al., 2007; Wacongne et al., 2011; Wang et al., 2015). Instead of merely storing each successive sound in a distinct memory slot (Baddeley, 2003; Baddeley & Hitch, 1974; Botvinick & Watanabe, 2007; Hurlstone et al., 2014), behavioral and brain imaging results suggest that participants mentally compressed these sequences using an algorithmic-like description where sequence regularities are expressed in terms of recursive combinations of simple rules (Al Roumi et al., 2021; Dehaene et al., 2015; Planton et al., 2021). Consistently with the predictions of this formal language of thought (LoT), behavioral performance and brain responses were modulated by the minimal description length (MDL) of the sequence, which we term LoT complexity. We discuss those points in turn.

Behavioral results during fMRI fully replicated our previously behavioral work (Planton et al., 2021). First, performance in detecting occasional deviants, thus indexing sequence memory, was strongly modulated by minimal description length in our formal language (LoT complexity; Figure 2A top). Second, even when a deviant was correctly detected, response time was strongly correlated with LoT complexity (Figure 2A bottom). Both findings indicate that novelty detection mechanisms were impacted by sequence structure. Finally, after the experiment, when participants were asked to segment the sequences with brackets, their segmentations closely matched the LoT sequence descriptions. For instance, they segmented

785 the *Pairs+Alt.1* sequence as [[AA][BB]][[ABAB]]. The sole exception was the alternate
786 sequence (ABAB…) which was encoded by our theory as 15 alternations, but was bracketed
787 by participants as 8 repetitions of the subsequence AB. This interesting departure from our
788 theory may indicate that, during sequence parsing, participants do not necessarily identify the
789 most compact representation, but wait until a repeated subsequence occurs, and then encode
790 how often it repeats (including nested repetitions). This parsing strategy would yield a minor
791 departure from our proposed encodings. Undoubtedly, there is still room for improvement in
792 our LoT theory, which is highly idealized and does not incorporate real-time parsing
793 constraints. However, an alternative interpretation of the bracketing results is that the visual
794 bracketing task itself may bias the perception of auditory sequences. By making the entire
795 sequence visible at once, including its start and end point, the visual format may have incited
796 subjects to subdivide it into groups of two, while the auditory sequential presentation alone
797 would have encouraged the "15 alternations" encoding. In support of the latter interpretation,
798 we did not find any evidence for grouping by two in the timing of button presses when subjects
799 reproduced the alternate sequence from memory (Al Roumi & Tabbane, unpublished data).
800 More research, with a greater diversity of sequences and tasks, will be needed to understand
801 whether and where the present theory needs to be amended.

802 Altogether, these behavioral results confirm that the postulated LoT provides a plausible
803 description of how binary sequences are encoded. They fit with a long line of cognitive
804 psychological research searching for computer-like languages that capture the human concept
805 of sequence regularity (Leeuwenberg, 1969; Restle, 1970; Restle & Brown, 1970; Simon, 1972;
806 Simon & Kotovsky, 1963). Here, as in Planton et al. (2021), a formal statistical comparison
807 demonstrated the superiority of LoT complexity against many competing measures such as
808 transition probability, chunk complexity, entropy, subsymmetries, Lempel-Ziv compression,
809 change complexity or algorithmic complexity. In the next sections, we discuss how brain
810 imaging results provide additional information on how sequence compression is implemented
811 in the human brain.

812 According to our hypothesis, the more complex the sequence, the longer the internal model
813 and the larger the effort to parse it, encode it and maintain it in working memory.
814 Consequently, we expected during the habituation phase larger brain activations for more
815 complex sequences in regions that are involved in auditory sequence encoding. Both fMRI and

816 MEG results supported this hypothesis. Importantly, contrary to the fMRI experiment, the
817 MEG experiment did not require overt responses, yet several neural markers, such as Global
818 Field Power, showed a significant increase with sequence complexity (Figure 6A).
819 Furthermore, linear regressions showed that brain activity increased with sequence
820 complexity for sensors that corresponded to the auditory and inferior frontal regions (Figure
821 6B).
822 Many levels of sequence processing mechanisms coexist in the human brain (Dehaene et al.,
823 2015) and statistical learning is a well-known contributor to brain activity. Thanks to the high
824 temporal resolution of MEG, we could separate the effects of transition probabilities from
825 those of sequence structure (Bekinschtein et al., 2009; Maheu et al., 2019; Wacongne et al.,
826 2011). To separate them, we ran a linear multilinear regression model with regressors for
827 both. Even after adding four additional regressions for immediate and longer-term transition
828 statistics, a cluster-based permutation test provided similar spatio-temporal clusters for the
829 regressor for LoT complexity (figure S6 and S7). As shown in Figure S8, for habituation and
830 standard trials, repetition/alternation impacted on both an early peak at 80ms and a later one
831 at 170 ms after stim onset, perhaps reflecting sensory bottom-up versus top-down processes.
832 Transition-based surprise exhibited only one peak at ~110 ms after stim onset. The 20ms delay
833 between the peaks supports the possibility that the first reflects low-level neural adaptation
834 while the second corresponds to a violation of expectations based on transition probabilities.
835 Complexity effects, however, showed a later and more sustained response, extending much
836 beyond 200 ms for deviant trials, in agreement with a distinct rule-based process.

837 Previous fMRI results led us to expect several prefrontal regions to exhibit an increasing
838 activity with sequence complexity (Badre, 2008; Badre et al., 2010; Barascud et al., 2016;
839 Koechlin et al., 2003; Koechlin & Jubault, 2006; Wang et al., 2019), but no such activation was
840 observed in MEG source reconstruction. This negative result has several potential
841 explanations. First of all, sequence complexity may act as a context effect and therefore may
842 be sustained across time (Barascud et al., 2016; Southwell & Chait, 2018). As we baselined the
843 data on a short time-window before each sound onset, such a constant effect may be
844 removed. Furthermore, frontal brain regions may be too distributed, intermixed and/or too
845 far from the MEG helmet to be faithfully reconstructed. Finally, the fMRI experiment allowed
846 us to clearly identify a large network of brain areas involved in complexity, but recruiting a

847 rather posterior region of prefrontal cortex, the preCG (or dorsal premotor cortex, PMd,
848 bordering on the dorsal part of Brodmann area 44) together with the STG, SMA, cerebellum,
849 and IPS that all exhibited the predicted increase in activity with LoT complexity. All these
850 regions showed the predicted increasing response with complexity during habituation, and
851 decreasing response with complexity to deviants.

852 All these areas have been shown to be associated with temporal sequence processing,
853 although mostly with oddball paradigms using much shorter or simpler sequences
854 (Bekinschtein et al., 2009; Huettel et al., 2002; Planton & Dehaene, 2021; Wang et al., 2015,
855 2019). They can be decomposed into modality-specific and modality-independent regions
856 (Frost et al., 2015). STG activation was observed for auditory sequences here and in other
857 work (Bekinschtein et al., 2009; Wang et al., 2015) but not visuo-spatial ones (Wang et al.,
858 2019). The modality specificity of STG was explicitly confirmed by Planton and Dehaene (2021)
859 using visual and auditory sequences with identical structures. Other regions, meanwhile, were
860 modality-independent and coincided with those found in a similar paradigm with visuo-spatial
861 sequences (Wang et al., 2019), consistent with a role in abstract rule formation. The IPS and
862 preCG, in particular, are jointly activated in various conditions of mental calculation and
863 mathematics (Amalric & Dehaene, 2017; Dehaene et al., 2003), with anterior IPS housing a
864 modality-invariant representation of number (Dehaene et al., 2003; Eger et al., 2009; Harvey
865 et al., 2013; Kanayet et al., 2018). The overlap between auditory sequences and arithmetic
866 was confirmed here using sensitive single-subject analyses (Figure 5). PreCG and IPS may thus
867 be jointly involved in the nested "for i=1:n" loops, i.e. the repetitions of the proposed
868 language, and in the real-time tracking of item and chunk number needed to follow a given
869 auditory sequence even after it was learned. Such a role is consistent with the more general
870 proposal of a role for these dorsal regions, particularly the intraparietal sulcus, in structure
871 learning (Summerfield et al., 2020). While these regions coactivated with STG during the
872 present auditory task, in a previous visuo-spatial version of the same task they did so together
873 with bilateral occipito-parietal areas (Wang et al., 2019). This is consistent with the behavioral
874 observation that the very same language, involving concatenation, loops and recursion, when
875 applied to distinct visual and auditory primitives, can account for sequence memory in both
876 modalities (Dehaene et al., 2022; Planton et al., 2021).

877 Our data also point to the SMA, or rather pre-SMA (Nachev et al., 2008), in processing
878 increasingly complex sequences. Such a domain-general sequence processing function was
879 indeed advocated by Cona & Semenza (2017) given its various involvements in action
880 sequences, music processing, numerical cognition, spatial processing, time processing, as well
881 as language. Remarkably, the cerebellum also participated in our complexity network. Its role
882 in working memory has been rarely reported or discussed and might have been
883 underestimated in the parsing of non-motor sequences, as it is classically associated with
884 motor sequence learning (Jenkins et al., 1994; Toni et al., 1998). The present results confirm
885 that the cerebellum may be involved in abstract, non-motor sequence encoding and
886 expectation (Leggio et al., 2008; Molinari et al., 2008; Nixon, 2003). Indeed, cerebellum, SMA
887 and premotor cortex were already reported as involved in the passive listening of rhythms (J.
888 L. Chen et al., 2008), consistent with a role in the identification of sequence regularities. A
889 tentative hypothesis is that (pre)SMA, cerebellum and possibly premotor cortex may
890 participate in a beat- (Morillon & Baillet, 2017) or time-processing network (Coull et al., 2011),
891 thus possibly involved in the translation from the abstract structures of the proposed language
892 to concrete, precisely timed sensory predictions.

893 Interestingly, we found that, while task performance was primarily linearly related to LoT
894 complexity, fMRI activity was not. Rather, as the sequence becomes too complex, activation
895 tended to stop increasing, or even decreased, just yielding a significant downward quadratic
896 trend. Wang et al. (2019) observed a similar effect with visuo-spatial sequences. In both cases,
897 the highest complexity sequences were largely incompressible because they did not have any
898 significant regularity in our language and, given their length, could not be easily memorized.
899 The collapse of activity at a certain level of LoT complexity, in regions that are precisely
900 involved in working memory, is therefore logical. Indeed, in a more classical object memory
901 task, Vogel and Machizawa (2004) found that working memory activity does not solely
902 increase with the number of elements stored in working memory, but saturates or decreases
903 once the stimuli exceed storage capacity, thought to be around three or four items (Cowan,
904 2001; for discussion, see Ma et al., 2014). Naturally, such a collapse can only lead to reduced
905 predictions and therefore reduced violation detection – thus explaining that behavioral
906 responses to deviants continue to increase linearly with complexity, while model-related fMRI
907 activations vary as an inverted U function of complexity. An analogous phenomenon was

908 described in infants (Kidd et al., 2012, 2014): they allocate their attention to visually or
909 auditory presented sequences that are neither too simple nor too complex, thus showing a U-
910 shaped pattern that implies boredom for stimuli with low information content and saturation
911 from stimuli that exceed their cognitive resources.

912 Detailed examination of the responses to violations in MEG confirmed that human
913 participants were able to encode details of the hierarchical structures of sequences. Not only
914 did the amplitude of violation responses tightly track the proposed LoT complexity (Figure 7),
915 but the specific violation responses proved that the human brain changed its expectations in
916 a hierarchical manner (Figure 8). This was clearest in the case of the Pairs+Alt1 sequence,
917 which consists in 2 pairs (AABB) followed by 4 alternations (ABAB). In those two consecutive
918 parts, the predictions are exactly opposite at central locations (A**AB**B versus A**BA**B), such that
919 what is a violation for one is a correct prediction for the other, and vice-versa. The fact that
920 we observe significant violation responses at each of these locations (i.e. locations 10, 12, 14
921 and 15 in the pairs+alt1 sequence), as well as for the matched *Alternate* and *Pairs* sequences,
922 indicates that the human brain is able to quickly change its anticipations as a function of
923 sequence hierarchical structure. To do so, it must contain a representation of sequences as
924 nested parts within parts, and switch between those parts after a fixed number of items (4 in
925 this case). Violation detection in the *Pairs* and *Quadruplets* sequences further confirmed that
926 subjects kept track of the exact number of items in each subsequence, since their brain
927 reacted to violations that either shortened or lengthened a chunk of identical consecutive
928 items.

929 While present and past results thus indicate that a language is necessary to account for the
930 human encoding of binary auditory sequences (Dehaene et al., 2022; Planton et al., 2021), this
931 language appears to differ from those used for communication, since it involves repetitions,
932 numbers and symmetries, while the syntax of natural language systematically avoids these
933 features (Moro, 1997; Musso et al., 2003). In agreement with this observation, there was little
934 overlap between our auditory sequence complexity network and the classical left-hemisphere
935 language network. Instead, complexity effects were systematically distributed symmetrically
936 in both hemispheres, unlike natural language processing. Within individually-defined language
937 fROIs (defined by their activity during visual or auditory sentence processing relative to a low-
938 level control), no significant complexity effect was found except in a single region, the left

IFGoper (a negative effect of complexity for deviants was also found there and in pSTS). Even that finding may well be a partial volume effect, as this area was absent from whole-brain contrasts, and the centroid of the complexity-related activation was centered at a more dorsal location in preCG (Figure 3). Broca's area is the main candidate region for language-like processing of hierarchical structures, and such role is advocated for in various previous rule-learning studies using artificial grammars (Bahlmann et al., 2008; Fitch & Friederici, 2012; Friederici et al., 2006), structured sequences of actions (Badre & D'Esposito, 2007; Koechlin & Jubault, 2006), sequence processing (Wang et al., 2015), and even music (Maess et al., 2001; Patel, 2003). However, Broca's area is a heterogeneous region (Amunts et al., 2010), of which certain sub-regions support language while others underlie a variety of other cognitive functions, including mathematics and working memory (Fedorenko et al., 2012). Interpretation must remain careful since functions that were once thought to overlap in Broca's area, such as language and musical syntax (Fadiga et al., 2009; Koelsch et al., 2002; Kunert et al., 2015), are now clearly dissociated by higher-resolution single-subject analyses (X. Chen et al., 2021).

Conversely, a very different picture was observed when examining the overlap of LoT complexity fMRI activity and the mathematical calculation network. There was considerable overlap at the whole-brain level (SMA, IPS, premotor cortex, cerebellum) and, most importantly, a significant sequence complexity effect within each of the individual mathematical fROIs. A similar result was reported by Wang et al. (2019); they found activation of mathematics-related regions but not language-related ones when participants were processing visuo-spatial sequences. Planton and Dehaene (2021) reached a similar conclusion by showing novelty effects to pattern violations of both visual and auditory short sequences in mathematics but not in language areas. Since their data, as well as the present data, was obtained with binary sequences which, contrary to Wang et al. (2019) were devoid of any geometrical content, those results indicate that the amodal language of thought for sequences shares common neural mechanisms with mathematical thinking, even when no overt geometrical content is present.

The present results therefore support the hypothesis that the human brain hosts multiple internal languages, depending on the types of structures and contents that are being processed (Dehaene et al., 2022; Fedorenko & Varley, 2016; Hagoort, 2013). While the

capacity to encode nested sequences may well be a fundamental overarching function of the human brain, fundamental to the manipulation of hierarchical structures in language, mathematics, music, complex actions, etc. (Dehaene et al., 2015; Fitch, 2014; Hauser et al., 2002; Lashley, 1951), those abilities may rely on partially dissociable networks. This conclusion fits with much prior evidence that, at the individual level, language and mathematics do not share the same cerebral substrates and may be dissociated by brain injuries (Amalric & Dehaene, 2016, 2017; Fedorenko & Varley, 2016), just like language and music (J. L. Chen et al., 2008; Norman-Haignere et al., 2015; Peretz et al., 2015). During hominization, we speculate that an enhanced functionality for recursive nesting may have jointly emerged in all of those neuronal circuits (Dehaene et al., 2022). In the future, this hypothesis could be tested by submitting non-human primates to the present hierarchy of sequences, and examine up to which level their brains can react to violations. We already know that the macaque monkey brain can detect violations of simple habitual, sequential or numerical patterns (Uhrig et al., 2014; Wilson et al., 2013), with both convergence (Wilson et al., 2017) and divergence (Wang et al., 2015) relative to human results. The present design may help determine precisely where to draw the line.

Materials and methods

Participants

Nineteen participants (10 men, M_{age} = 27.6 years, SD_{age} = 4.7 years) took part in the MEG experiment and twenty-three (11 men, M_{age} = 26.1 years, SD_{age} = 4.7 years) in the fMRI experiment. The two groups of participants were distinct. We did not test any effect of gender on the results of this study. All participants had normal or corrected to normal vision and no history or indications of psychological or neurological disorders. In compliance with institutional guidelines, all subjects gave written informed consent prior to enrollment and received 90€ as compensation. The experiments were approved by the national ethical committees (CPP Ile-de-France III and CPP Sud-Est VI).

Stimuli and tasks

Auditory binary sequences of 16 sounds were used in both experiments. They were composed of low pitch and high pitch sounds, constructed as the superimposition of sinusoidal signals of respectively f = 350Hz, 700Hz and 1400Hz, and f = 500Hz, 1000Hz and 2000Hz. Each tone lasted 50 ms and the 16 tones were presented in sequence with a fixed SOA of 250ms.

Ten 16-items sequential patterns spanning a large range of complexities were selected (see Figure 1A). Six of them were used in previous behavioral experiments (Planton et al., 2021). The complexity metric used to predict behavior and brain activity was the "Language-of-thought – *chunk*" complexity, which was previously shown to be well correlated with behavior (Planton et al., 2021). This metric roughly measures the length of the shortest description of the pattern in a formal language that uses a small set of atomic rules (e.g. repetition, alternation) that can be recursively embedded. The *chunk* version of the metric includes only expressions that preserve chunks of consecutive repeated items (for instance, the sequence ABBA is parsed as [A][BB][A] rather than [AB][BA]). 10 sequences were used in the fMRI experiment, and 7 of them in the MEG experiment (i.e. all but *Pairs&Alt.2*, *ThreeTwo* and *CenterMirror*).

Each auditory sequence (4000 ms long) was repeatedly presented to a participant in a mini-session with 500 ms ITI. Mini-sessions had the following structure. Participants first

1015 discovered and encoded the sequence during a habituation phase of 10 trials. Then, during a
1016 test phase, occasional violations consisting in the replacement of a high pitch sound by a low
1017 pitch one (or vice-versa) were presented at the locations specified in Figure 1A. As described
1018 in Figure 1B, in the MEG experiment, the test phase included 36 trials of which 2/3 comprised
1019 a deviant sound. In the fMRI experiment, the test phase included 18 trials of which 1/3
1020 comprised a deviant sound. Participants were unaware of the mini-session structure.

1021 In the MEG experiment, habituation and test sequences followed each other
1022 seamlessly, and participants were merely asked to listen attentively. After each mini-session,
1023 they were asked one general question about what they had just heard such as: *How many*
1024 *different sounds could you hear? Did you find it musical? How complex was the sequence of*
1025 *sounds?* The full experiment was divided temporally into 2 parts such that the 7 sequence
1026 types appeared twice, once in each version (starting with A or B), once at the beginning and
1027 once at the end of the experiment. The overall experiment lasted about 80 minutes.

1028 In the fMRI experiment, participants were explicitly instructed to detect and respond
1029 to violations, by pressing a button, as quickly as possible, with either their right or left hand.
1030 The correct response button (left or right, counterbalanced over the two repetitions of each
1031 sequence) was indicated by a 2s visual message on the screen during the rest period preceding
1032 the first test trial. In order to optimize the estimation of the BOLD response, trials were
1033 presented in two blocks of 5 trials for the habituation phase, then three blocks of 6 trials for
1034 the test phase, separated by rest periods of variable duration (6s ± 1.5). The 10 sequences
1035 appeared twice, once in each version (starting with A or B). The 20 mini-sessions were
1036 presented across 5 fMRI sessions of approximately 11 minutes.

1037 Post-experimental sequence bracketing task

1038 After the experiment, participants were given a questionnaire to assess their own
1039 representation of the structure of the sequence. For each sequence of the experiment (i.e. 7
1040 for the MEG participants, 10 for the fMRI participants), after listening to it several times if
1041 needed, participants were asked to segment the sequence by drawing brackets (opening and
1042 closing) on its visual representation As and Bs were respectively represented by empty and
1043 filled circles on a sheet of paper). In this way, they were instructed to indicate how they tended
1044 to group consecutive items together in their mind when listening to the sequence, if they did.

1045 ## fMRI experiment procedures

1046 ### Localizer session

1047 Together with the main sequence processing task described above, the fMRI
1048 experimental protocol also included a 6-min localizer session designed to localize cerebral
1049 regions involved in language processing and in mathematics. This localizer was already used
1050 in our previous work (Planton & Dehaene, 2021) and is a variant of a previously published
1051 functional localizer which is fully described elsewhere (Pinel et al., 2007). A sentence
1052 processing network was identified in each subject by contrasting sentence reading/listening
1053 conditions (i.e. visually and auditorily presented sentences) from control conditions (i.e.
1054 meaningless auditory stimuli consisting in rotated sentences, and meaningless visual stimuli
1055 of the same size and visual complexity as visual words). A mathematics network was identified
1056 in each subject by contrasting mental calculation conditions (i.e. mental processing of simple
1057 subtraction problems, such as 7 − 2, presented visually, and auditorily) from sentence
1058 reading/listening conditions.

1059 ### fMRI acquisition and preprocessing

1060 MRI acquisition was performed on a 3T scanner (Siemens, Tim Trio), equipped with a
1061 64-channel head coil. 354 functional scans covering the whole brain were acquired for each
1062 of the 5 sessions of the main experiment, as well as 175 functional scans for the localizer
1063 session, all using a T2*-weighted gradient echo-planar imaging (EPI) sequence (69 interleaved
1064 slices, TR = 1.81 s, TE = 30.4 ms, voxel size = 1.75 mm3, multiband factor = 3). To estimate
1065 distortions, two volumes with opposite phase encoding direction were acquired: one volume
1066 in the anterior to posterior direction (AP) and one volume in the other direction (PA). A 3D T1-
1067 weighted structural image was also acquired (TR = 2.30 s, TE = 2.98 ms, voxel size = 1.0 mm3).
1068 Data processing (except the TOPUP correction) was performed with SPM12 (Wellcome
1069 Department of Cognitive Neurology, http://www.fil.ion.ucl.ac.uk/spm). The anatomical scan
1070 was spatially normalized to a standard Montreal Neurological Institute (MNI) reference
1071 anatomical template brain using the default parameters. Functional images were unwarped
1072 (using the AP/PA volumes, processed with the TOPUP software; FSL, fMRIB), corrected for slice
1073 timing differences (first slice as reference), realigned (registered to the mean using 2nd degree
1074 B-Splines), coregistered to the anatomy (using Normalized Mutual Information), spatially

1075 normalized to the MNI brain space (using the parameters obtained from the normalization of
1076 the anatomy), and smoothed with an isotropic Gaussian filter of 5-mm FWHM.
1077 In addition to the 6 motion regressors from the realignment step, 12 regressors were
1078 computed using the aCompCor method (Behzadi et al., 2007), applied to the CSF and to white
1079 matter (first 5 components of two principal component analyses, and 1 for the raw signal), in
1080 order to better correct for motion-related and physiological noise in the statistical models
1081 (using the PhysIO Toolbox Kasper et al., 2017). Additional regressors for motion outliers were
1082 also computed (framewise displacement larger than 0.5 mm; see Power et al., 2012), they
1083 represented 0.5% of volumes per subject on average. One participant was excluded from the
1084 fMRI analyses due to excessive movement in the scanner (average translational displacement
1085 of 2.9 mm within each fMRI session, which was 3.3 SD above group average).

1086 **fMRI analysis**

1087 *General linear model*

1088 Statistical analyses were performed using SPM12 and general linear models (GLM) that
1089 included the motion-related and physiological noise-related regressors (described above) as
1090 covariates of no interest. fMRI images were high-pass filtered at 0.01 Hz. Time series from the
1091 sequences of stimuli of each condition (each tone modeled as an event) were convolved with
1092 the canonical hemodynamic response function (HRF). Specifically, for each of the twenty mini-
1093 sessions (i.e. each sequence being tested twice, reverting the attribution of the two tones),
1094 one regressor for the items of the habituation phase, one for the items of the test phase and
1095 one for the deviant items were included in the GLM. Since motor responses and deviant trials
1096 were highly collinear, manual motor responses were not modeled. However, motor responses
1097 could be less frequent for more complex sequences (i.e. increased miss rate), thus creating a
1098 potential confound with the effect of complexity in deviant trials. We thus also computed an
1099 alternative model in which only correctly-detected deviants trials were included. In order to
1100 test for a relationship between brain activation and LoT complexity in different trial types (i.e.
1101 habituation trials, deviant trials), corresponding beta maps for each of the 10 sequences and
1102 each participant were entered in second-level within-subject ANOVA analyses. Linear
1103 parametric contrasts using the LoT complexity value were then computed.

1104 *Cross-validated ROI plots and analyses*

1105 To further test the reliability of the complexity effect across participants, a cross-
1106 validated region-of-interest (ROI) analysis, using individually-defined functional ROIs (fROIs),
1107 was conducted. Nine of the most salient peaks from the positive LoT complexity contrast in
1108 habituation were first selected, and used to build nine 20-mm-diameter spherical search
1109 volumes: supplementary motor area (SMA; coordinates: -1, 5, 65), right precentral gyrus (R-
1110 preCG; 46, 2, 44), left precentral gyrus (L-preCG; -47, 0, 45), right intraparietal sulcus (R-IPS;
1111 36, -46, 56), left intraparietal sulcus (L-IPS; -31, -42, 44), right superior temporal gyrus (R-STG;
1112 48, -32, 3), left superior temporal gyrus (L-STG; -68, -23, 5), lobule VI of the left cerebellar
1113 hemisphere (L-CER6; -29, -56, -28) and lobule VI of the right cerebellar hemisphere (R-CER8;
1114 22, -68, -51).). Since these search volumes were defined on group-level results, to reduce to
1115 degree of circularity when extracting the individual ROI data, these were extracted in a cross-
1116 validated manner, by separating each participant data into two halves. Individual fROIs were
1117 then defined for each participant by selecting the 20% most active voxels at the intersection
1118 between each search volume and the contrast "LoT complexity effect in habituation"
1119 computed on half of the blocks (i.e. blocks of sequences starting with "A"). Mean contrast
1120 estimates for each fROI and each condition was then extracted using the other half of the
1121 blocks (i.e. blocks of sequences starting with "B"). The same procedure was repeated a second
1122 time by reversing the role of the two halves (i.e. fROIs computed using blocks of sequences
1123 starting with "B", data extracted from blocks of sequences starting with "A"). It should be
1124 noted that this procedure does not fully eliminate the circularity in the analysis, since the
1125 initial search volumes were still based on whole-group data – however, such circularity should
1126 be minimal, as the ROIs themselves. To test for the significance of the complexity effect in
1127 each ROI, the mean of the output of the two procedures (i.e. the cross-validated activation
1128 value), for each of the ten conditions (i.e. habituation blocks for each of the 10 sequences)
1129 and each participant, was entered in a linear mixed-effect model with participant as random
1130 factor and LoT complexity value as a fixed-effect predictor. P values were corrected for
1131 multiple comparison using Bonferroni correction for nine ROIs. Along with such a linear effect
1132 of complexity, we also tested a quadratic effect by adding a quadratic term in the mixed-effect
1133 model.

1134 In order to track activation over time, we also extracted, using the same cross validated
1135 procedure, the BOLD activation time course for each 28-trials mini-session. To account for the

1136 fact that the duration of rest periods between blocks could vary, data were actually extracted
1137 for a [-6s – 32s] period relative to the onset of the first trial of each block rest period, and the
1138 whole mini-session curve was recomposed by averaging over the overlapping period of two
1139 consecutive parts (see vertical shadings in Figure 3B). Each individual time course was
1140 upsampled and smoothed using cubic spline interpolation, and baseline-corrected with a 6-
1141 seconds period preceding the onset of the first trial.

1142 Finally, two set of ROIs were selected in order to test for the involvement of language
1143 and mathematics-related areas in the present sequence processing task, and especially to
1144 assess a potential sequence complexity effect. Seven language-related ROIs came from the
1145 sentence processing experiment of Pallier et al. (2011): pars orbitalis (IFGorb), triangularis
1146 (IFGtri), and opercularis (IFGoper) of the inferior frontal gyrus, temporal pole (TP),
1147 temporoparietal junction (TPJ), anterior superior temporal sulcus (aSTS) and posterior
1148 superior temporal sulcus (pSTS). Seven mathematics-related ROIs came from the
1149 mathematical thinking experiment of Amalric & Dehaene (2016): left and right intraparietal
1150 sulcus (IPS), left and right superior frontal gyrus (SFG), left and right precentral/inferior frontal
1151 gyrus (preCG/IFG), supplementary motor area (SMA). These two set of ROIs were already used
1152 in the past (Planton & Dehaene, 2021; Wang et al., 2019). In order to build individual and
1153 functional ROIs from these literature-based ROIs, we used the same procedure as Planton &
1154 Dehaene (2021) consisting in selecting, for each subject, the 20% most active voxels within
1155 the intersection between the ROI mask and an fMRI contrast of interest from the independent
1156 localizer session. The contrast of interest was "Listening & reading sentences > Rotated speech
1157 & false font script" for the ROIs of the language network, and "Mental calculation visual &
1158 auditory > Sentence listening & reading" for the ROIs of the mathematics network. Mean
1159 contrast estimates for each fROI and each condition was then extracted, and entered into
1160 linear mixed model mixed effect model with participant as random factor and LoT complexity
1161 value as a fixed effect predictor. A Bonferonni correction for 14 ROIs was applied to the p
1162 values.

1163 ## Behavioral data analysis

1164 Data for the sequence bracketing task included all productions collected in the fMRI
1165 and MEG experiment (42 participants for seven sequences, and 23 participants for the three

that were only presented during fMRI). For each production, we counted the total number of brackets (opening and closing) drawn at each interval between two consecutive items (as well as before the first and after the last item, resulting in a vector of length 17) (see Figure 2A). To determine if participants' reported sequence structure matched the predictions of the LoT model, we computed the correlation between the average over participants of the number of brackets in each interval and the postulated bracketing of the sequence (derived from its expression in the LoT). For the first two sequences, the representations "[A][A][A]…" and "[AAA…]", as well as "[A][B][A]…" and "[ABA…]", respectively derived from the expressions [+0]^16 and [+0]^16<b>, were considered as equivalent.

For the violation detection task of the fMRI experiment, we considered as a correct response (or "hit") all button presses occurring between 200 ms and 2500 ms after the onset of a deviant sound. We thus allowed for potential delayed responses (but found that 97.7% of correct responses were below 1500 ms). An absence of response in this interval was counted as a miss, a button press outside this interval was counted as a false alarm. We then computed, for each subject and each sequence, the average response time as well as, using the proportions of hits and false alarms, the sensitivity (or d'). The method of Hautus (1995) was used to adjust extreme values. To test whether subject performance correlated with LoT complexity, we performed linear regressions on group-averaged data, as well linear mixed models including participant as the (only) random factor. The random effect structure of the mixed models was kept minimal, and did not include any random slopes, to avoid the convergence issues often encountered when attempting to fit more complex models. Analyses were performed in R 4.0.2 (R Core Team, 2020), using the lme4 (Bates et al., 2015) and lmerTest (Kuznetsova et al., 2017) packages. Surprise for each deviant item was computed from transition probabilities, within each block for each subject, using an ideal observer Bayesian model (Maheu et al., 2019; Meyniel et al., 2016) and tested as an additional predictor in the mixed effect models. For the analysis of d', we used the average surprise of the deviant items of the block (i.e. all deviants presented to the subject, whether or not they detected them). For the analysis of response times, we used the average transition-based surprise of the correctly-detected deviant items of the block

MEG experiment procedures

MEG recordings

Participants listened to the sequences while sitting inside an electromagnetically shielded room. The magnetic component of their brain activity was recorded with a 306-channel, whole-head MEG by Elekta Neuromag® (Helsinki, Finland). 102 triplets, each comprising one magnetometer and two orthogonal planar gradiometers composed the MEG helmet. The brain signals were acquired at a sampling rate of 1000 Hz with a hardware highpass filter at 0.1Hz. The data was then resampled at 250 Hz.

Eye movements and heartbeats were monitored with vertical and horizontal electro-oculograms (EOGs) and electrocardiograms (ECGs). Head shape was digitized using various points on the scalp as well as the nasion, left and right pre-auricular points (FASTTRACK, Polhemus). Subjects' head position inside the helmet was measured at the beginning of each run with an isotrack Polhemus Inc. system from the location of four coils placed over frontal and mastoïdian skull areas. Sounds were presented using Eatymotic audio system (an HiFi-quality artifact-free headphone system with wide frequency response) while participants had to fixate a central cross. The analysis was performed with MNE Python (Gramfort et al., 2013; Jas et al., 2018), version 0.23.0.

Data cleaning: Maxfiltering

We applied the signal space separation algorithm *mne.preprocessing.maxwell_filter* (Taulu et al., 2004) to suppress magnetic signals from outside the sensor helmet and interpolate bad channels that we identified visually in the raw signal and in the power spectrum. This algorithm also compensated for head movements between experimental blocks by realigning all data to an average head position.

Data cleaning: ICA

Oculomotor and cardiac artefacts were removed performing an independent component analysis (ICA) on the four last runs of the experiment. The components that correlated the most with the EOG and ECG signals were automatically detected. We then visually inspected their topography and correlation to the ECG and EOG time series to confirm their rejection from the MEG data. A maximum of 1 component for the cardiac artefact and 2

components for the ocular artefacts were considered. Finally, we removed them from the whole recording (14 runs).

Data cleaning: Autoreject

We used an automated algorithm for rejection and repair of bad trials (Jas et al., 2017) that computes the optimal peak-to-peak threshold per channel-type in a cross-validated manner. It was applied to baselined epochs and removed on average 4.6% of the epochs.

Epoching parameters and projection on magnetometers

Epochs on items were baselined from -50 ms to 0 ms (stimulus onset) and epochs on the full sequences were baselined between -200ms to 0ms (first sequence item onset). For sensor level analyses, instead of working with the 306 sensors (102 magnetometers and 206 gradiometers), we projected the spherical sources of signal onto the magnetometers using MNE epochs method *epochs.as_type('mag',mode='accurate').*

Univariate analyses

GFP and linear regressions

Global field power was computed as the root-mean-square of evoked responses or the difference of evoked responses. Linear regressions were computed using 4-fold cross-validation and with the *linear_model.LinearRegression* function of scikit-learn package version 0.24.1. Pearson correlation was computed with the *stats.pearsonr* function from *scipy* package. The predictors for surprise from transition probabilities were computed using an ideal observer Bayesian model learning first-order transitions with an exponential memory decay over 100 items. This was done thanks to the TransitionProbModel python package, which is the python version of the *Matlab version* used in (Maheu et al., 2019; Meyniel et al., 2016).

Source reconstruction

A T1-weighted anatomical MRI image with 1 mm isometric resolution was acquired for each participant (3T Prisma Siemens scanner). The anatomical MRI was segmented with FreeSurfer (Dale et al., 1999; Fischl et al., 2002) and co-registered with MEG data in MNE using the digitized markers. A three-layer boundary element model (inner skull, outer skull and outer skin) was used to estimate the current-source density distribution over the cortical surface. Source reconstruction was performed on the linear regression coefficients using the

1254 dSPM solution with MNE default values (loose orientation of 0.2, depth weighting of 0.8, SNR
1255 value of 3) (Dale et al., 2000). The noise covariance matrix used for data whitening was
1256 estimated from the signal within the 200 ms preceding the onset of the first item of each
1257 sound sequence. The resulting sources estimates were transformed to a standard anatomical
1258 template (*fsaverage*) with 20484 vertices using the MNE morphing procedure, and averaged
1259 across subjects.

1260 **Multivariate analyses**

1261 Data was smoothed with a 100 ms sliding window and, instead of working with the 306
1262 sensors (102 magnetometers and 206 gradiometers), we projected the spherical sources of
1263 signal onto the magnetometers using MNE epochs method
1264 *epochs.as_type('mag',mode='accurate').*
1265

1266 *Time-resolved multivariate decoding of brain responses to standard and deviant sounds*

1267 The goal of multivariate of time-resolved decoding analyses was to predict from single-
1268 trial brain activity (*X*) a specific categorical variable (*y*), namely if the trial corresponded to the
1269 presentation of a deviant sound or not. These analyses were performed using MNE-python
1270 function *GeneralizingEstimator* from version 0.23.0 (Gramfort et al., 2013) and with Scikit-
1271 learn package version 1.1.1 (Pedregosa et al., 2011). Prior to model fitting, channels were z-
1272 scored across trials for every time-point. The estimator was fitted on each participant
1273 separately, across all MEG sensors using the parameters set to their default values provided
1274 by the Scikit-Learn package (Pedregosa et al., 2011).

1275 *Cross-validation*

1276 One run was dedicated to each version of the sequence (7 sequence types x 2 versions
1277 [starting with A or starting with B] = 14 runs). To build the training set, we randomly picked
1278 one run for each sequence, irrespectively of the sequence version. We trained the decoder on
1279 all deviant trials of the 7 sequences and on standard trials (non-deviant trials from the test
1280 phase) that were matched to sequence-specific deviants in ordinal position. We then tested
1281 this decoder on the remaining 7 blocks, determining its performance for the 7 sequences
1282 separately. The training and the testing sets were then inverted, resulting in a 2-folds cross-

validation. This procedure avoided any confound with item identity, as the sounds A and B were swapped in the cross-validation folds.

Generalization across time

To access the temporal organization of the neural representations, we computed the generalization-across-time (GAT) matrices (King & Dehaene, 2014). These matrices represent the decoding score of an estimator trained at time t (training time on the vertical axis) and tested with data from another time t' (testing time on the horizontal axis).

Statistical analyses

Temporal, spatiotemporal and temporal-temporal cluster-based permutation tests were computed on the time-windows of interest (0-350ms for habituation and standard items and 0-600ms for deviants) using *stats.permutation_cluster_1samp_test* from MNE python package. To obtain the significance results presented in Figure 8, we ran the temporal permutation test on the difference between the predictions of the deviancy decoder for standard and deviant sounds for a time-window from 0 to 600 ms after deviant onset. To compute spatiotemporal clusters, we provided the function with an adjacency matrix from *mne.channels.find_ch_connectivity.*

Reference

Aksentijevic, A., & Gibson, K. (2012). Complexity equals change. *Cognitive Systems Research*, *15–16*, 1–16. https://doi.org/10.1016/j.cogsys.2011.01.002

Al Roumi, F., Marti, S., Wang, L., Amalric, M., & Dehaene, S. (2021). Mental compression of spatial sequences in human working memory using numerical and geometrical primitives. *Neuron*, *109*(16), 2627-2639.e4. https://doi.org/10.1016/j.neuron.2021.06.009

Alexander, C., & Carey, S. (1968). Subsymmetries. *Perception & Psychophysics*, *4*(2), 73–77. https://doi.org/10.3758/BF03209511

Amalric, M., & Dehaene, S. (2016). Origins of the brain networks for advanced mathematics in expert mathematicians. *Proceedings of the National Academy of Sciences*, *113*(18), 4909–4917. https://doi.org/10.1073/pnas.1603205113

Amalric, M., & Dehaene, S. (2017). Cortical circuits for mathematical knowledge: Evidence for a major subdivision within the brain's semantic networks. *Philosophical Transactions of the Royal Society B: Biological Sciences*, *373*(1740), 20160515–20160515. https://doi.org/10.1098/rstb.2016.0515

Amalric, M., Wang, L., Pica, P., Figueira, S., Sigman, M., & Dehaene, S. (2017). The language of geometry: Fast comprehension of geometrical primitives and rules in human adults and preschoolers. *PLOS Computational Biology*, *13*(1), e1005273. https://doi.org/10.1371/journal.pcbi.1005273

Amunts, K., Lenzen, M., Friederici, A. D., Schleicher, A., Morosan, P., Palomero-Gallagher, N., & Zilles, K. (2010). Broca's region: Novel organizational principles and multiple receptor mapping. *PLoS Biol*, *8*(9). https://doi.org/10.1371/journal.pbio.1000489

Baddeley, A. (2003). Working memory: Looking back and looking forward. *Nature Reviews Neuroscience*, *4*(10), Article 10. https://doi.org/10.1038/nrn1201

Baddeley, A. D., & Hitch, G. (1974). Recent advances in learning and motivation. In *Working Memory, Vol. 8,*.

Badre, D. (2008). Cognitive control, hierarchy, and the rostro-caudal organization of the frontal lobes. *Trends in Cognitive Sciences*. https://doi.org/10.1016/j.tics.2008.02.004

Badre, D., & D'Esposito, M. (2007). Functional Magnetic Resonance Imaging Evidence for a Hierarchical Organization of the Prefrontal Cortex. *Journal of Cognitive Neuroscience*, *19*(12), 2082–2099. https://doi.org/10.1162/jocn.2007.19.12.2082

Badre, D., Kayser, A. S., & D'Esposito, M. (2010). Frontal Cortex and the Discovery of Abstract Action Rules. *Neuron*, *66*(2), 315–326. https://doi.org/10.1016/j.neuron.2010.03.025

Bahlmann, J., Schubotz, R. I., & Friederici, A. D. (2008). Hierarchical artificial grammar processing engages Broca's area. *NeuroImage*, *42*(2), 525–534. https://doi.org/10.1016/j.neuroimage.2008.04.249

Barascud, N., Pearce, M. T., Griffiths, T. D., Friston, K. J., & Chait, M. (2016). Brain

responses in humans reveal ideal observer-like sensitivity to complex acoustic patterns. *Proceedings of the National Academy of Sciences*, *113*(5), E616–E625. https://doi.org/10.1073/pnas.1508523113

Bates, D., Mächler, M., Bolker, B., & Walker, S. (2015). Fitting Linear Mixed-Effects Models Using lme4. *Journal of Statistical Software*, *67*, 1–48. https://doi.org/10.18637/jss.v067.i01

Behzadi, Y., Restom, K., Liau, J., & Liu, T. T. (2007). A component based noise correction method (CompCor) for BOLD and perfusion based fMRI. *NeuroImage*, *37*(1), 90–101. https://doi.org/10.1016/j.neuroimage.2007.04.042

Bekinschtein, T. A., Dehaene, S., Rohaut, B., Tadel, F., Cohen, L., & Naccache, L. (2009). Neural signature of the conscious processing of auditory regularities. *Proceedings of the National Academy of Sciences*, *106*(5), 1672–1677. https://doi.org/10.1073/pnas.0809667106

Bendixen, A., Roeber, U., & Schröger, E. (2007). Regularity extraction and application in dynamic auditory stimulus sequences. *Journal of Cognitive Neuroscience*, *19*(10), 1664–1677. https://doi.org/10.1162/jocn.2007.19.10.1664

Bendixen, A., Schröger, E., & Winkler, I. (2009). I Heard That Coming: Event-Related Potential Evidence for Stimulus-Driven Prediction in the Auditory System. *The Journal of Neuroscience*, *29*(26), 8447–8451. https://doi.org/10.1523/JNEUROSCI.1493-09.2009

Bhanji, J. P., Beer, J. S., & Bunge, S. A. (2010). Taking a gamble or playing by the rules: Dissociable prefrontal systems implicated in probabilistic versus deterministic rule-based decisions. *NeuroImage*, *49*(2), 1810–1819. https://doi.org/10.1016/j.neuroimage.2009.09.030

Botvinick, M., & Watanabe, T. (2007). From numerosity to ordinal rank: A gain-field model of serial order representation in cortical working memory. *Journal of Neuroscience*, *27*(32), 8636–8642. https://doi.org/10.1523/JNEUROSCI.2110-07.2007

Buiatti, M., Peña, M., & Dehaene-Lambertz, G. (2009). Investigating the neural correlates of continuous speech computation with frequency-tagged neuroelectric responses. *NeuroImage*, *44*(2), 509–519. https://doi.org/10.1016/j.neuroimage.2008.09.015

Chao, Z. C., Takaura, K., Wang, L., Fujii, N., & Dehaene, S. (2018). Large-Scale Cortical Networks for Hierarchical Prediction and Prediction Error in the Primate Brain. *Neuron*, *100*(5), 1252-1266.e3. https://doi.org/10.1016/j.neuron.2018.10.004

Chater, N., & Vitányi, P. (2003). Simplicity: A unifying principle in cognitive science? *Trends in Cognitive Sciences*, *7*(1), 19–22. https://doi.org/10.1016/S1364-6613(02)00005-0

Chen, J. L., Penhune, V. B., & Zatorre, R. J. (2008). Listening to musical rhythms recruits motor regions of the brain. *Cerebral Cortex (New York, N.Y.: 1991)*, *18*(12), 2844–2854. https://doi.org/10.1093/cercor/bhn042

Chen, X., Affourtit, J., Ryskin, R., Regev, T. I., Norman-Haignere, S., Jouravlev, O., Malik-Moraleda, S., Kean, H., Varley, R., & Fedorenko, E. (2021). *The human language system does not support music processing* (p. 2021.06.01.446439). https://doi.org/10.1101/2021.06.01.446439

Cona, G., & Semenza, C. (2017). Supplementary motor area as key structure for domain-

general sequence processing: A unified account. *Neuroscience and Biobehavioral Reviews*, *72*, 28–42. https://doi.org/10.1016/j.neubiorev.2016.10.033

Coull, J. T., Cheng, R.-K., & Meck, W. H. (2011). Neuroanatomical and Neurochemical Substrates of Timing. *Neuropsychopharmacology*, *36*(1), Article 1. https://doi.org/10.1038/npp.2010.113

Cowan, N. (2001). The magical number 4 in short-term memory: A reconsideration of mental storage capacity. *Behavioral and Brain Sciences*, *24*(1), 87–114. https://doi.org/10.1017/S0140525X01003922

Cowan, N. (2010). The Magical Mystery Four: How Is Working Memory Capacity Limited, and Why? *Current Directions in Psychological Science*, *19*(1), 51–57. https://doi.org/10.1177/0963721409359277

Dale, A. M., Fischl, B., & Sereno, M. I. (1999). Cortical surface-based analysis. I. Segmentation and surface reconstruction. *NeuroImage*, *9*(2), 179–194. https://doi.org/10.1006/nimg.1998.0395

Dale, A. M., Liu, A. K., Fischl, B. R., Buckner, R. L., Belliveau, J. W., Lewine, J. D., & Halgren, E. (2000). Dynamic statistical parametric mapping: Combining fMRI and MEG for high-resolution imaging of cortical activity. *Neuron*, *26*(1), 55–67. https://doi.org/10.1016/s0896-6273(00)81138-1

Dehaene, S., Al Roumi, F., Lakretz, Y., Planton, S., & Sablé-Meyer, M. (2022). Symbols and mental programs: A hypothesis about human singularity. *Trends in Cognitive Science*, *in press*.

Dehaene, S., Meyniel, F., Wacongne, C., Wang, L., & Pallier, C. (2015). The Neural Representation of Sequences: From Transition Probabilities to Algebraic Patterns and Linguistic Trees. *Neuron*, *88*(1), 2–19. https://doi.org/10.1016/j.neuron.2015.09.019

Dehaene, S., Piazza, M., Pinel, P., & Cohen, L. (2003). Three parietal circuits for number processing. *Cognitive Neuropsychology*, *20*, 487–506.

Delahaye, J.-P., & Zenil, H. (2012). Numerical evaluation of algorithmic complexity for short strings: A glance into the innermost structure of randomness. *Applied Mathematics and Computation*, *219*(1), 63–77. https://doi.org/10.1016/j.amc.2011.10.006

Eger, E., Michel, V., Thirion, B., Amadon, A., Dehaene, S., & Kleinschmidt, A. (2009). Deciphering cortical number coding from human brain activity patterns. *Curr Biol*, *19*(19), 1608–1615. https://doi.org/10.1016/j.cub.2009.08.047

El Karoui, I., King, J.-R., Sitt, J., Meyniel, F., Van Gaal, S., Hasboun, D., Adam, C., Navarro, V., Baulac, M., Dehaene, S., Cohen, L., & Naccache, L. (2015). Event-Related Potential, Time-frequency, and Functional Connectivity Facets of Local and Global Auditory Novelty Processing: An Intracranial Study in Humans. *Cerebral Cortex*, *25*(11), 4203–4212. https://doi.org/10.1093/cercor/bhu143

Fadiga, L., Craighero, L., & D'Ausilio, A. (2009). Broca's area in language, action, and music. *Ann N Y Acad Sci*, *1169*, 448–458. https://doi.org/10.1111/j.1749-6632.2009.04582.x

Fedorenko, E., Duncan, J., & Kanwisher, N. (2012). Language-selective and domain-general regions lie side by side within Broca's area. *Current Biology: CB*, *22*(21), 2059–2062. https://doi.org/10.1016/j.cub.2012.09.011

Fedorenko, E., & Varley, R. (2016). Language and thought are not the same thing: Evidence from neuroimaging and neurological patients. *Annals of the New York Academy of Sciences*, *1369*(1), 132–153. https://doi.org/10.1111/nyas.13046

Feldman, J. (2000). Minimization of Boolean complexity in human concept learning. *Nature*, *407*(6804), 630–633. https://doi.org/10.1038/35036586

Ferrigno, S., Cheyette, S. J., Piantadosi, S. T., & Cantlon, J. F. (2020). Recursive sequence generation in monkeys, children, U.S. adults, and native Amazonians. *Science Advances*, *6*(26), eaaz1002. https://doi.org/10.1126/sciadv.aaz1002

Fischl, B., Salat, D. H., Busa, E., Albert, M., Dieterich, M., Haselgrove, C., van der Kouwe, A., Killiany, R., Kennedy, D., Klaveness, S., Montillo, A., Makris, N., Rosen, B., & Dale, A. M. (2002). Whole brain segmentation: Automated labeling of neuroanatomical structures in the human brain. *Neuron*, *33*(3), 341–355. https://doi.org/10.1016/s0896-6273(02)00569-x

Fitch, W. T. (2004). Computational Constraints on Syntactic Processing in a Nonhuman Primate. *Science*, *303*(5656), 377–380. https://doi.org/10.1126/science.1089401

Fitch, W. T. (2014). Toward a computational framework for cognitive biology: Unifying approaches from cognitive neuroscience and comparative cognition. *Physics of Life Reviews*, *11*(3), 329–364. https://doi.org/10.1016/j.plrev.2014.04.005

Fitch, W. T., & Friederici, A. D. (2012). Artificial grammar learning meets formal language theory: An overview. *Philosophical Transactions of the Royal Society B: Biological Sciences*, *367*(1598), 1933–1955. https://doi.org/10.1098/rstb.2012.0103

Fitch, W. T., & Martins, M. D. (2014). Hierarchical processing in music, language, and action: Lashley revisited. *Annals of the New York Academy of Sciences*, *1316*, 87–104. https://doi.org/10.1111/nyas.12406

Fló, A., Brusini, P., Macagno, F., Nespor, M., Mehler, J., & Ferry, A. L. (2019). Newborns are sensitive to multiple cues for word segmentation in continuous speech. *Developmental Science*, *22*(4), e12802. https://doi.org/10.1111/desc.12802

Fodor, J. A. (1975). *The language of thought* (Vol. 5). Harvard university press.

Friederici, A. D., Bahlmann, J., Heim, S., Schubotz, R. I., & Anwander, A. (2006). The brain differentiates human and non-human grammars: Functional localization and structural connectivity. *Proceedings of the National Academy of Sciences of the United States of America*, *103*(7), 2458–2463. https://doi.org/10.1073/pnas.0509389103

Friston, K. (2005). A theory of cortical responses. *Philosophical Transactions of the Royal Society B: Biological Sciences*, *360*(1456), 815–836. https://doi.org/10.1098/rstb.2005.1622

Frost, R., Armstrong, B. C., Siegelman, N., & Christiansen, M. H. (2015). Domain generality versus modality specificity: The paradox of statistical learning. *Trends in Cognitive Sciences*, *19*(3), 117–125. https://doi.org/10.1016/j.tics.2014.12.010

Fujii, N., & Graybiel, A. M. (2003). Representation of action sequence boundaries by macaque prefrontal cortical neurons. *Science (New York, N.Y.)*, *301*(5637), 1246–1249. https://doi.org/10.1126/science.1086872

Gauvrit, N., Zenil, H., Delahaye, J.-P., & Soler-Toscano, F. (2014). Algorithmic complexity for short binary strings applied to psychology: A primer. *Behavior Research Methods*, *46*(3), 732–744. https://doi.org/10.3758/s13428-013-0416-0

Gentner, T. Q., Fenn, K. M., Margoliash, D., & Nusbaum, H. C. (2006). Recursive syntactic pattern learning by songbirds. *Nature*, *440*(7088), 1204–1207. https://doi.org/10.1038/nature04675

Glanzer, M., & Clark, W. H. (1963). Accuracy of perceptual recall: An analysis of organization. *Journal of Verbal Learning and Verbal Behavior*, *1*(4), 289–299. https://doi.org/10.1016/S0022-5371(63)80008-0

Gramfort, A., Luessi, M., Larson, E., Engemann, D. A., Strohmeier, D., Brodbeck, C., Goj, R., Jas, M., Brooks, T., Parkkonen, L., & Hämäläinen, M. (2013). MEG and EEG data analysis with MNE-Python. *Frontiers in Neuroscience*, *7*. https://doi.org/10.3389/fnins.2013.00267

Grunwald, P. (2004). A tutorial introduction to the minimum description length principle. *arXiv:Math/0406077*. http://arxiv.org/abs/math/0406077

Hagoort, P. (2013). MUC (Memory, Unification, Control) and beyond. *Frontiers in Psychology*, *4*. https://doi.org/10.3389/fpsyg.2013.00416

Harvey, B. M., Klein, B. P., Petridou, N., & Dumoulin, S. O. (2013). Topographic Representation of Numerosity in the Human Parietal Cortex. *Science*, *341*(6150), 1123–1126. https://doi.org/10.1126/science.1239052

Hauser, M. D., Chomsky, N., & Fitch, W. T. (2002). The Faculty of Language: What Is It, Who Has It, and How Did It Evolve? *Science*, *298*(5598), 1569–1579. https://doi.org/10.1126/science.298.5598.1569

Hauser, M. D., Newport, E. L., & Aslin, R. N. (2001). Segmentation of the speech stream in a non-human primate: Statistical learning in cotton-top tamarins. *Cognition*, *78*(3), B53-64. https://doi.org/10.1016/s0010-0277(00)00132-3

Hautus, M. J. (1995). Corrections for extreme proportions and their biasing effects on estimated values ofd′. *Behavior Research Methods, Instruments, & Computers*, *27*(1), 46–51. https://doi.org/10.3758/BF03203619

Heilbron, M., & Chait, M. (2018). Great Expectations: Is there Evidence for Predictive Coding in Auditory Cortex? *Neuroscience*, *389*, 54–73. https://doi.org/10.1016/j.neuroscience.2017.07.061

Huettel, S. A., Mack, P. B., & McCarthy, G. (2002). Perceiving patterns in random series: Dynamic processing of sequence in prefrontal cortex. *Nat Neurosci*, *5*(5), 485–490.

Hurlstone, M. J., Hitch, G. J., & Baddeley, A. D. (2014). Memory for serial order across domains: An overview of the literature and directions for future research. *Psychological*

Bulletin, *140*(2), 339. https://doi.org/10.1037/a0034221

Jas, M., Engemann, D. A., Bekhti, Y., Raimondo, F., & Gramfort, A. (2017). Autoreject: Automated artifact rejection for MEG and EEG data. *NeuroImage*, *159*, 417–429. https://doi.org/10.1016/j.neuroimage.2017.06.030

Jas, M., Larson, E., Engemann, D. A., Leppäkangas, J., Taulu, S., Hämäläinen, M., & Gramfort, A. (2018). A Reproducible MEG/EEG Group Study With the MNE Software: Recommendations, Quality Assessments, and Good Practices. *Frontiers in Neuroscience*, *12*. https://doi.org/10.3389/fnins.2018.00530

Jenkins, I. H., Brooks, D. J., Nixon, P. D., Frackowiak, R. S., & Passingham, R. E. (1994). Motor sequence learning: A study with positron emission tomography. *The Journal of Neuroscience: The Official Journal of the Society for Neuroscience*, *14*(6), 3775–3790.

Jiang, X., Long, T., Cao, W., Li, J., Dehaene, S., & Wang, L. (2018). Production of Supra-regular Spatial Sequences by Macaque Monkeys. *Current Biology: CB*, *28*(12), 1851-1859.e4. https://doi.org/10.1016/j.cub.2018.04.047

Kanayet, F. J., Mattarella-Micke, A., Kohler, P. J., Norcia, A. M., McCandliss, B. D., & McClelland, J. L. (2018). Distinct Representations of Magnitude and Spatial Position within Parietal Cortex during Number–Space Mapping. *Journal of Cognitive Neuroscience*, *30*(2), 200–218. https://doi.org/10.1162/jocn_a_01199

Karuza, E. A., Kahn, A. E., & Bassett, D. S. (2019). Human Sensitivity to Community Structure Is Robust to Topological Variation. *Complexity*, *2019*, e8379321. https://doi.org/10.1155/2019/8379321

Kasper, L., Bollmann, S., Diaconescu, A. O., Hutton, C., Heinzle, J., Iglesias, S., Hauser, T. U., Sebold, M., Manjaly, Z.-M., Pruessmann, K. P., & Stephan, K. E. (2017). The PhysIO Toolbox for Modeling Physiological Noise in fMRI Data. *Journal of Neuroscience Methods*, *276*, 56–72. https://doi.org/10.1016/j.jneumeth.2016.10.019

Kidd, C., Piantadosi, S. T., & Aslin, R. N. (2012). The Goldilocks effect: Human infants allocate attention to visual sequences that are neither too simple nor too complex. *PloS One*, *7*(5), e36399. https://doi.org/10.1371/journal.pone.0036399

Kidd, C., Piantadosi, S. T., & Aslin, R. N. (2014). The Goldilocks Effect in Infant Auditory Attention. *Child Development*, *85*(5), 1795–1804. https://doi.org/10.1111/cdev.12263

King, J. R., & Dehaene, S. (2014). Characterizing the dynamics of mental representations: The temporal generalization method. *Trends in Cognitive Sciences*, *18*(4), 203–210. https://doi.org/10.1016/J.TICS.2014.01.002

King, J. R., Faugeras, F., Gramfort, A., Schurger, A., El Karoui, I., Sitt, J. D., Rohaut, B., Wacongne, C., Labyt, E., Bekinschtein, T., Cohen, L., Naccache, L., & Dehaene, S. (2013). Single-trial decoding of auditory novelty responses facilitates the detection of residual consciousness. *NeuroImage*, *83*, 726–738. https://doi.org/10.1016/j.neuroimage.2013.07.013

Kóbor, A., Takács, Á., Kardos, Z., Janacsek, K., Horváth, K., Csépe, V., & Nemeth, D. (2018). ERPs differentiate the sensitivity to statistical probabilities and the learning of sequential structures during procedural learning. *Biological Psychology*, *135*, 180–193.

https://doi.org/10.1016/j.biopsycho.2018.04.001

Koechlin, E., & Jubault, T. (2006). Broca's Area and the Hierarchical Organization of Human Behavior. *Neuron*, *50*(6), 963–974. https://doi.org/10.1016/j.neuron.2006.05.017

Koechlin, E., Ody, C., & Kouneiher, F. (2003). The Architecture of Cognitive Control in the Human Prefrontal Cortex. *Science*, *302*(5648), 1181–1185. https://doi.org/10.1126/science.1088545

Koelsch, S., Gunter, T. C., von Cramon, D. Y., Zysset, S., Lohmann, G., & Friederici, A. D. (2002). Bach speaks: A cortical "language-network" serves the processing of music. *Neuroimage*, *17*(2), 956–966.

Kunert, R., Willems, R. M., Casasanto, D., Patel, A. D., & Hagoort, P. (2015). Music and Language Syntax Interact in Broca's Area: An fMRI Study. *PloS One*, *10*(11), e0141069. https://doi.org/10.1371/journal.pone.0141069

Kuznetsova, A., Brockhoff, P. B., & Christensen, R. H. B. (2017). lmerTest Package: Tests in Linear Mixed Effects Models. *Journal of Statistical Software*, *82*, 1–26. https://doi.org/10.18637/jss.v082.i13

Lashley, K. S. (1951). The problem of serial order in behavior. In *Cerebral mechanisms in behavior; the Hixon Symposium* (pp. 112–146). Wiley.

Leeuwenberg, E. L. (1969). Quantitative specification of information in sequential patterns. *Psychological Review*, *76*(2), 216.

Leggio, M. G., Tedesco, A. M., Chiricozzi, F. R., Clausi, S., Orsini, A., & Molinari, M. (2008). Cognitive sequencing impairment in patients with focal or atrophic cerebellar damage. *Brain: A Journal of Neurology*, *131*(Pt 5), 1332–1343. https://doi.org/10.1093/brain/awn040

Lempel, A., & Ziv, J. (1976). On the Complexity of Finite Sequences. *IEEE Transactions on Information Theory*, *22*(1), 75–81. https://doi.org/10.1109/TIT.1976.1055501

Li, M., & Vitányi, P. (1993). An Introduction to Kolmogorov Complexity and Its Applications. In *An Introduction to Kolmogorov Complexity and Its Applications*. Springer New York. https://doi.org/10.1007/978-1-4757-3860-5

Ma, W. J., Husain, M., & Bays, P. M. (2014). Changing concepts of working memory. *Nature Neuroscience*, *17*(3), Article 3. https://doi.org/10.1038/nn.3655

Maess, B., Koelsch, S., Gunter, T. C., & Friederici, A. D. (2001). Musical syntax is processed in Broca's area: An MEG study. *Nature Neuroscience*, *4*(5), Article 5. https://doi.org/10.1038/87502

Maheu, M., Dehaene, S., & Meyniel, F. (2019). Brain signatures of a multiscale process of sequence learning in humans. *eLife*, *8*, e41541. https://doi.org/10.7554/eLife.41541

Maheu, M., Meyniel, F., & Dehaene, S. (2021). *Rational arbitration between statistics and rules in human sequence processing* (p. 2020.02.06.937706). bioRxiv. https://doi.org/10.1101/2020.02.06.937706

Mathy, F., & Feldman, J. (2012). What's magic about magic numbers? Chunking and data compression in short-term memory. *Cognition*, *122*(3), 346–362. https://doi.org/10.1016/j.cognition.2011.11.003

May, P. J., & Tiitinen, H. (2010). Mismatch negativity (MMN), the deviance-elicited auditory deflection, explained. *Psychophysiology*, *47*(1), 66–122. https://doi.org/10.1111/j.1469-8986.2009.00856.x

Mazoyer, B., Zago, L., Mellet, E., Bricogne, S., Etard, O., Houdé, O., Crivello, F., Joliot, M., Petit, L., & Tzourio-Mazoyer, N. (2001). Cortical networks for working memory and executive functions sustain the conscious resting state in man. *Brain Research Bulletin*, *54*(3), 287–298. https://doi.org/10.1016/s0361-9230(00)00437-8

McDermott, J. H., Schemitsch, M., & Simoncelli, E. P. (2013). Summary statistics in auditory perception. *Nature Neuroscience*, *16*(4), Article 4. https://doi.org/10.1038/nn.3347

Meyer, T., & Olson, C. R. (2011). Statistical learning of visual transitions in monkey inferotemporal cortex. *Proceedings of the National Academy of Sciences*, *108*(48), 19401–19406. https://doi.org/10.1073/pnas.1112895108

Meyniel, F., Maheu, M., & Dehaene, S. (2016). Human Inferences about Sequences: A Minimal Transition Probability Model. *PLOS Computational Biology*, *12*(12), e1005260. https://doi.org/10.1371/journal.pcbi.1005260

Miller, G. A. (1956). The magical number seven, plus or minus two: Some limits on our capacity for processing information. *Psychological Review*, *63*(2), 81–97. https://doi.org/10.1037/h0043158

Molinari, M., Chiricozzi, F. R., Clausi, S., Tedesco, A. M., De Lisa, M., & Leggio, M. G. (2008). Cerebellum and Detection of Sequences, from Perception to Cognition. *The Cerebellum*, *7*(4), 611–615. https://doi.org/10.1007/s12311-008-0060-x

Morillon, B., & Baillet, S. (2017). Motor origin of temporal predictions in auditory attention. *Proceedings of the National Academy of Sciences*, *114*(42), E8913–E8921. https://doi.org/10.1073/pnas.1705373114

Moro, A. (1997). Dynamic Antisymmetry: Movement as a Symmetry-breaking Phenomenon. *Studia Linguistica*, *51*(1), 50–76. https://doi.org/10.1111/1467-9582.00017

Musso, M., Moro, A., Glauche, V., Rijntjes, M., Reichenbach, J., Buchel, C., & Weiller, C. (2003). Broca's area and the language instinct. *Nat Neurosci*, *6*(7), 774–781.

Näätänen, R., Paavilainen, P., Alho, K., Reinikainen, K., & Sams, M. (1989). Do event-related potentials reveal the mechanism of the auditory sensory memory in the human brain? *Neuroscience Letters*, *98*(2), 217–221. https://doi.org/10.1016/0304-3940(89)90513-2

Nachev, P., Kennard, C., & Husain, M. (2008). Functional role of the supplementary and pre-supplementary motor areas. *Nature Reviews Neuroscience*, *9*(11), Article 11. https://doi.org/10.1038/nrn2478

Nixon, P. D. (2003). The role of the cerebellum in preparing responses to predictable sensory events. *The Cerebellum*, *2*(2), 114. https://doi.org/10.1080/14734220309410

Norman-Haignere, S., Kanwisher, N. G., & McDermott, J. H. (2015). Distinct Cortical Pathways for Music and Speech Revealed by Hypothesis-Free Voxel Decomposition. *Neuron*, *88*(6), 1281–1296. https://doi.org/10.1016/j.neuron.2015.11.035

Pallier, C., Devauchelle, A.-D., & Dehaene, S. (2011). Cortical representation of the constituent structure of sentences. *Proceedings of the National Academy of Sciences*, *108*(6), 2522–2527. https://doi.org/10.1073/pnas.1018711108

Patel, A. D. (2003). Language, music, syntax and the brain. *Nature Neuroscience*, *6*(7), Article 7. https://doi.org/10.1038/nn1082

Pedregosa, F., Varoquaux, G., Gramfort, A., Michel, V., Thirion, B., Grisel, O., Blondel, M., Prettenhofer, P., Weiss, R., Dubourg, V., Vanderplas, J., Passos, A., Cournapeau, D., Brucher, M., Perrot, M., & Duchesnay, É. (2011). Scikit-learn: Machine learning in Python. *Journal of Machine Learning Research*, *12*, 2825–2830.

Peretz, I., Vuvan, D., Lagrois, M.-É., & Armony, J. L. (2015). Neural overlap in processing music and speech. *Philosophical Transactions of the Royal Society B: Biological Sciences*, *370*(1664), 20140090. https://doi.org/10.1098/rstb.2014.0090

Pinel, P., Thirion, B., Meriaux, S., Jobert, A., Serres, J., Le Bihan, D., Poline, J.-B., & Dehaene, S. (2007). Fast reproducible identification and large-scale databasing of individual functional cognitive networks. *BMC Neuroscience*, *8*, 91. https://doi.org/10.1186/1471-2202-8-91

Planton, S., & Dehaene, S. (2021). Cerebral representation of sequence patterns across multiple presentation formats. *Cortex*, *145*, 13–36. https://doi.org/10.1016/j.cortex.2021.09.003

Planton, S., van Kerkoerle, T., Abbih, L., Maheu, M., Meyniel, F., Sigman, M., Wang, L., Figueira, S., Romano, S., & Dehaene, S. (2021). A theory of memory for binary sequences: Evidence for a mental compression algorithm in humans. *PLOS Computational Biology*, *17*(1), e1008598. https://doi.org/10.1371/journal.pcbi.1008598

Power, J. D., Barnes, K. A., Snyder, A. Z., Schlaggar, B. L., & Petersen, S. E. (2012). Spurious but systematic correlations in functional connectivity MRI networks arise from subject motion. *NeuroImage*, *59*(3), 2142–2154. https://doi.org/10.1016/j.neuroimage.2011.10.018

Psotka, J. (1975). Simplicity, symmetry, and syntely: Stimulus measures of binary pattern structure. *Memory & Cognition*, *3*(4), 434–444. https://doi.org/10.3758/BF03212938

Raichle, M. E. (2015). The brain's default mode network. *Annual Review of Neuroscience*, *38*, 433–447. https://doi.org/10.1146/annurev-neuro-071013-014030

Restle, F. (1970). Theory of serial pattern learning: Structural trees. *Psychological Review*, *77*(6), 481–495. https://doi.org/10.1037/h0029964

Restle, F., & Brown, E. R. (1970). Serial pattern learning: Pretraining of runs and trills. *Psychonomic Science*, *19*(6), 321–322.

Sablé-Meyer, M., Ellis, K., Tenenbaum, J., & Dehaene, S. (2022). A language of thought for

the mental representation of geometric shapes. *Cognitive Psychology*, *139*, 101527. https://doi.org/10.1016/j.cogpsych.2022.101527

Saffran, J. R., Aslin, R. N., & Newport, E. L. (1996). Statistical Learning by 8-Month-Old Infants. *Science*. https://doi.org/10.1126/science.274.5294.1926

Sakai, K., Kitaguchi, K., & Hikosaka, O. (2003). Chunking during human visuomotor sequence learning. *Experimental Brain Research*, *152*(2), 229–242. https://doi.org/10.1007/s00221-003-1548-8

Santolin, C., & Saffran, J. R. (2018). Constraints on Statistical Learning Across Species. *Trends in Cognitive Sciences*, *22*(1), 52–63. https://doi.org/10.1016/j.tics.2017.10.003

Schapiro, A. C., Rogers, T. T., Cordova, N. I., Turk-Browne, N. B., & Botvinick, M. M. (2013). Neural representations of events arise from temporal community structure. *Nature Neuroscience*, *16*(4), Article 4. https://doi.org/10.1038/nn.3331

Schröger, E., Bendixen, A., Trujillo-Barreto, N. J., & Roeber, U. (2007). Processing of abstract rule violations in audition. *PloS One*, *2*(11), e1131. https://doi.org/10.1371/journal.pone.0001131

Shima, K., Isoda, M., Mushiake, H., & Tanji, J. (2007). Categorization of behavioural sequences in the prefrontal cortex. *Nature*, *445*(7125), 315–318. https://doi.org/10.1038/nature05470

Simon, H. A. (1972). Complexity and the representation of patterned sequences of symbols. *Psychological Review*, *79*(5), 369.

Simon, H. A., & Kotovsky, K. (1963). Human acquisition of concepts for sequential patterns. *Psychological Review*, *70*(6), 534.

Southwell, R., & Chait, M. (2018). Enhanced deviant responses in patterned relative to random sound sequences. *Cortex*, *109*, 92–103. https://doi.org/10.1016/j.cortex.2018.08.032

Summerfield, C., & de Lange, F. P. (2014). Expectation in perceptual decision making: Neural and computational mechanisms. *Nature Reviews Neuroscience*, *15*(11), 745–756. https://doi.org/10.1038/nrn3838

Summerfield, C., Luyckx, F., & Sheahan, H. (2020). Structure learning and the posterior parietal cortex. *Progress in Neurobiology*, *184*, 101717. https://doi.org/10.1016/j.pneurobio.2019.101717

Taulu, S., Kajola, M., & Simola, J. (2004). Suppression of interference and artifacts by the signal space separation method. *Brain Topography*, *16*(4), 269–275. https://doi.org/10.1023/B:BRAT.0000032864.93890.f9

Todorovic, A., Ede, F. van, Maris, E., & Lange, F. P. de. (2011). Prior Expectation Mediates Neural Adaptation to Repeated Sounds in the Auditory Cortex: An MEG Study. *Journal of Neuroscience*, *31*(25), 9118–9123. https://doi.org/10.1523/JNEUROSCI.1425-11.2011

Todorovic, A., & Lange, F. P. de. (2012). Repetition Suppression and Expectation Suppression Are Dissociable in Time in Early Auditory Evoked Fields. *Journal of*

Neuroscience, *32*(39), 13389–13395. https://doi.org/10.1523/JNEUROSCI.2227-12.2012

Toni, I., Krams, M., Turner, R., & Passingham, R. E. (1998). The time course of changes during motor sequence learning: A whole-brain fMRI study. *NeuroImage*, *8*(1), 50–61. https://doi.org/10.1006/nimg.1998.0349

Toro, J. M., & Trobalón, J. B. (2005). Statistical computations over a speech stream in a rodent. *Perception & Psychophysics*, *67*(5), 867–875. https://doi.org/10.3758/BF03193539

Uhrig, L., Dehaene, S., & Jarraya, B. (2014). A Hierarchy of Responses to Auditory Regularities in the Macaque Brain. *Journal of Neuroscience*, *34*(4), 1127–1132. https://doi.org/10.1523/JNEUROSCI.3165-13.2014

van Heijningen, C. A. A., de Visser, J., Zuidema, W., & ten Cate, C. (2009). Simple rules can explain discrimination of putative recursive syntactic structures by a songbird species. *Proceedings of the National Academy of Sciences*, *106*(48), 20538–20543. https://doi.org/10.1073/pnas.0908113106

Vitz, P. C., & Todd, T. C. (1969). A coded element model of the perceptual processing of sequential stimuli. *Psychological Review*, *76*(5), 433–449. https://doi.org/10.1037/h0028113

Vogel, E. K., & Machizawa, M. G. (2004). Neural activity predicts individual differences in visual working memory capacity. *Nature*, *428*(6984), 748–751. https://doi.org/10.1038/nature02447

Vul, E., Harris, C., Winkielman, P., & Pashler, H. (2009). Puzzlingly High Correlations in fMRI Studies of Emotion, Personality, and Social Cognition. *Perspectives in Psychological Science*, *4*(3), 274–290.

Wacongne, C., Changeux, J.-P., & Dehaene, S. (2012). A Neuronal Model of Predictive Coding Accounting for the Mismatch Negativity. *Journal of Neuroscience*, *32*(11), 3665–3678. https://doi.org/10.1523/JNEUROSCI.5003-11.2012

Wacongne, C., Labyt, E., van Wassenhove, V., Bekinschtein, T., Naccache, L., & Dehaene, S. (2011). Evidence for a hierarchy of predictions and prediction errors in human cortex. *Proc Natl Acad Sci U S A*, *108*(51), 20754–20759. https://doi.org/10.1073/pnas.1117807108

Wang, L., Amalric, M., Fang, W., Jiang, X., Pallier, C., Figueira, S., Sigman, M., & Dehaene, S. (2019a). Representation of spatial sequences using nested rules in human prefrontal cortex. *NeuroImage*, *186*, 245–255. https://doi.org/10.1016/j.neuroimage.2018.10.061

Wang, L., Amalric, M., Fang, W., Jiang, X., Pallier, C., Figueira, S., Sigman, M., & Dehaene, S. (2019b). Representation of spatial sequences using nested rules in human prefrontal cortex. *NeuroImage*, *186*, 245–255. https://doi.org/10.1016/j.neuroimage.2018.10.061

Wang, L., Uhrig, L., Jarraya, B., & Dehaene, S. (2015). Representation of Numerical and Sequential Patterns in Macaque and Human Brains. *Current Biology*, *25*(15), 1966–1974. https://doi.org/10.1016/j.cub.2015.06.035

Wilson, B., Marslen-Wilson, W. D., & Petkov, C. I. (2017). Conserved Sequence Processing in Primate Frontal Cortex. *Trends in Neurosciences*, *40*(2), 72–82. https://doi.org/10.1016/j.tins.2016.11.004

Wilson, B., Slater, H., Kikuchi, Y., Milne, A. E., Marslen-Wilson, W. D., Smith, K., & Petkov, C. I. (2013). Auditory Artificial Grammar Learning in Macaque and Marmoset Monkeys. *Journal of Neuroscience*, *33*(48), 18825–18835. https://doi.org/10.1523/JNEUROSCI.2414-13.2013

Sequences	LoT Description	Verbal Description
Repeat	[+0]^16	16 repetitions
Alternate	+0,[b]^15	15 alternations
Pairs	[[+0]^2]^8<b>	8 pairs
Quadruplets	[[+0]^4]^4<b>	4 quadruplets
Pairs&Alt.1	[[[+0]^2]^2<b>,[b]^4]^2<+0>	2 pairs then 4 alternations, repeated twice
Shrinking	[[+0]^4]^2<b>,[[b]^2<+0>]^2,[b]^4	2 quadruplets then 2 pairs then 4 alternations
Pairs&Alt.2*	[+0,b,[[b]^2<+0>]^2,[b]^2]^2<+0>	A tone then the other then 2 pairs then 2 alternations
ThreeTwo*	[[+0]^3,[b]^2<+0>,b,[b]^2<+0>]^2<+0>	A triplet then a pair then a tone then a pair, repeated twice
CenterMirror*	[+0]^4,[b]^2<+0>,[b]^4,[b]^2<+0>, [b]^4<+0>	A quadruplet then a pair then 4 alternations then a pair then a quadruplet
Complex	+0,b,[b]^3<+0>,[b]^4<+0>,b, [b]^2<+0>,[b]^3<+0>,b	A tone then a tone then a triplet then a quadruplet then a tone then a pair then a triplet then a tone

Figure S1. Selected sequences. The first column indicates the list of the different 16-items sequences used in the MEG and fMRI experiments, with associated LoT complexity. *Sequences used only in the fMRI experiment. The second column provides the sequence description obtained from the LoT. The third column is its verbal description, meant to ease the understanding of the formal expression.

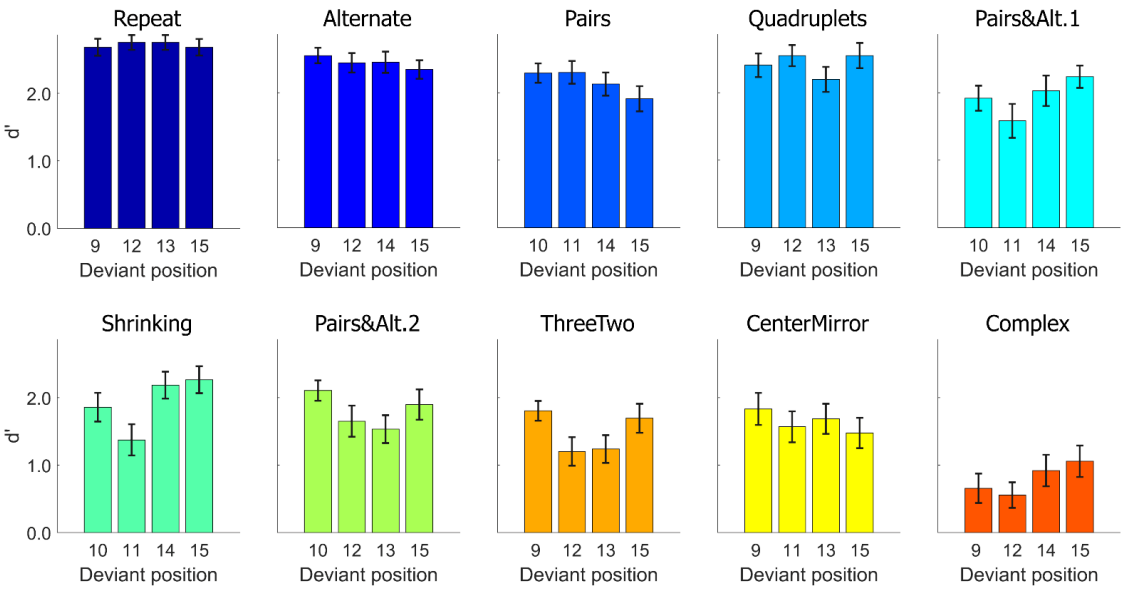

Figure S2. Task performance: average sensitivity (d'), for each position and each sequence. Error bars represent SEM.

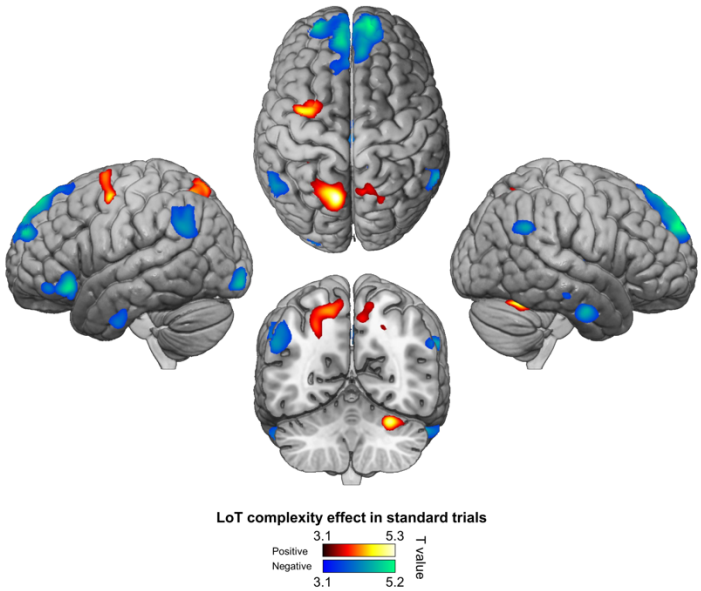

Figure S3. Positive (hot colors) and negative (cold colors) effects of LoT complexity effects on standard trials (voxel-wise p < .001, uncorrected; cluster-wise p < .05, FDR corrected).

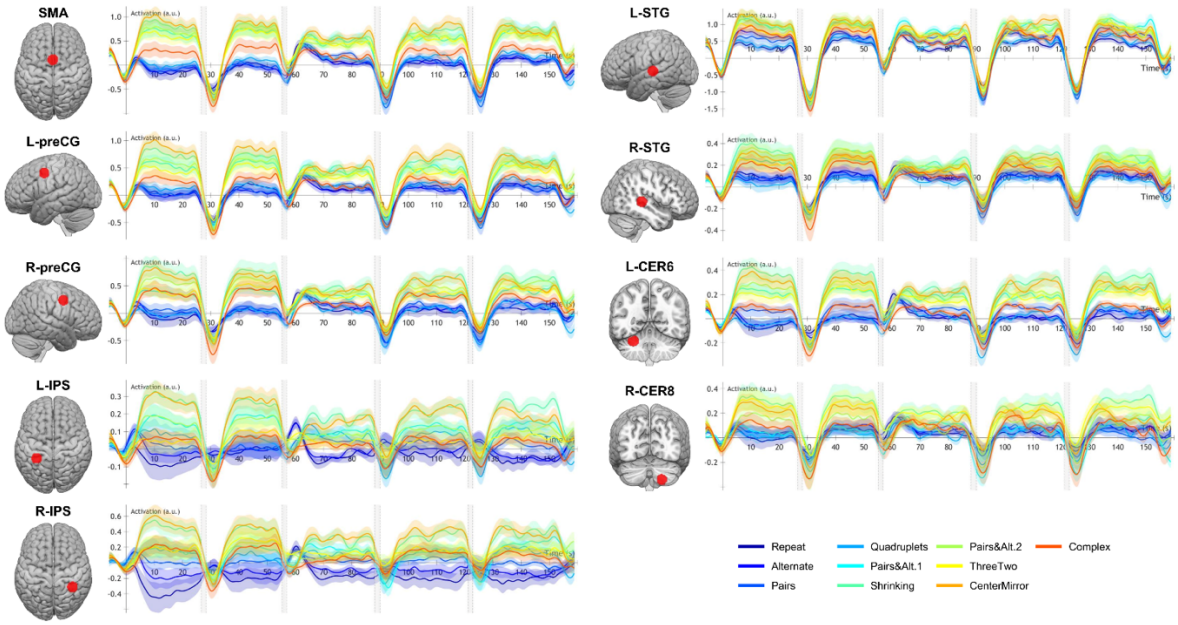

Figure S4. Time course of group-averaged BOLD signals for each sequence in nine ROIs where a LoT complexity effect was found. Each mini-session lasted 160-seconds and was composed of 5 blocks (2 habituation and 3 tests) interspersed with short rest periods of variable duration (depicted in light gray). The full time course was reconstituted by resynchronizing the data at the onset of each successive block (see Methods). Shading around each time course represents one SEM.

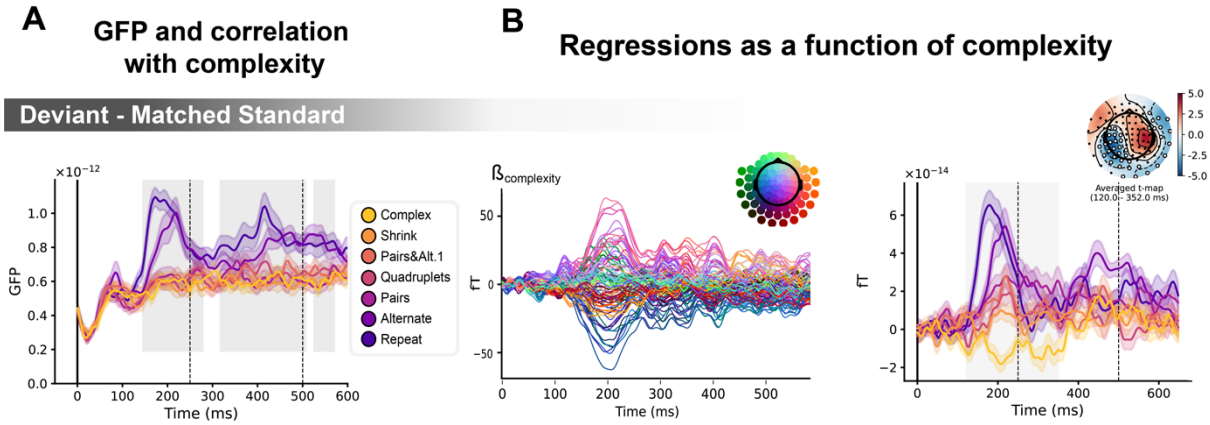

Figure S5. Sequence complexity modulates the contrast of Deviant – Matched Standard trials. A) Global field power computed for the Deviant – Matched Standard contrast for each sequence (see color legend). 0 ms indicates sound onset. Significant correlation with sequence complexity is indicated by the shaded areas. **B)** Regressions of contrast as a function of sequence complexity. Left: amplitude of the regression coefficients ß of the complexity regressor for each MEG sensor. Right: spatiotemporal clusters where regression coefficients were significantly different from 0. Two clusters were found, the sake of illustration, only one is shown here. Unsurprisingly, the clusters involved the same sensors as in Figure 6. Neural signals were averaged over significant sensors for each sequence type and were plotted separately.

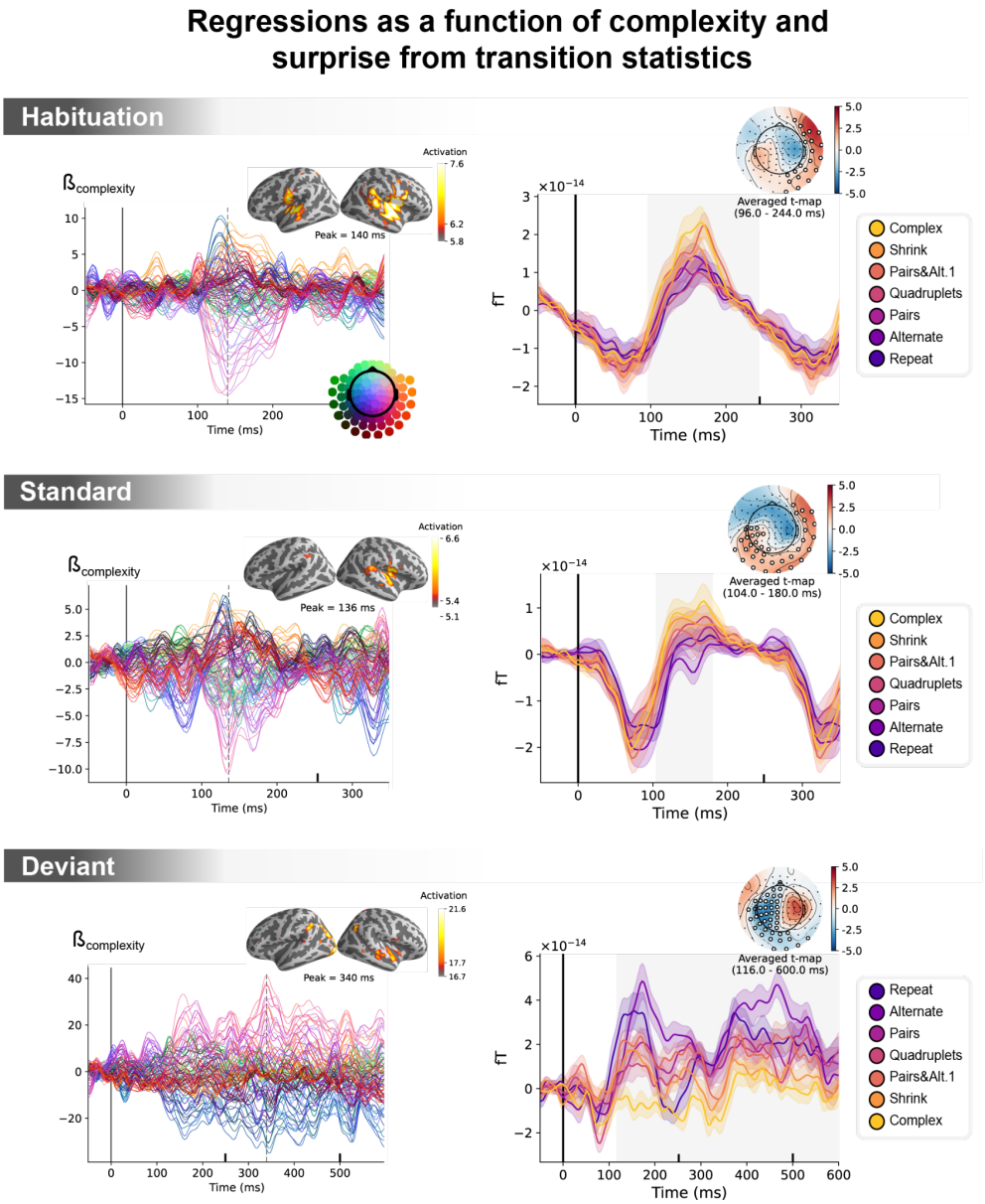

Figure S6 Unconfounding the effects of statistical surprise and sequence complexity on MEG signals. Left: amplitude of the regression coefficients ß of the complexity regressor for each MEG sensor, in a general linear model where transition-based surprise, repetition and alternation were also modeled. Insets show the projection of these coefficients on the source space for its maximal amplitude value, indicated by the vertical dotted lines. Right: illustration of spatiotemporal clusters where regression coefficients were significantly different from 0. The time windows identified by the permutation test are indicated by the shaded areas and have an opposite T-value for *Deviant* trials. Neural signals were averaged over the cluster sensors for each sequence type and were plotted separately (see color legend). Note that the time-window goes until 600 ms for *Deviant* trials and until 350 ms for the other trials.

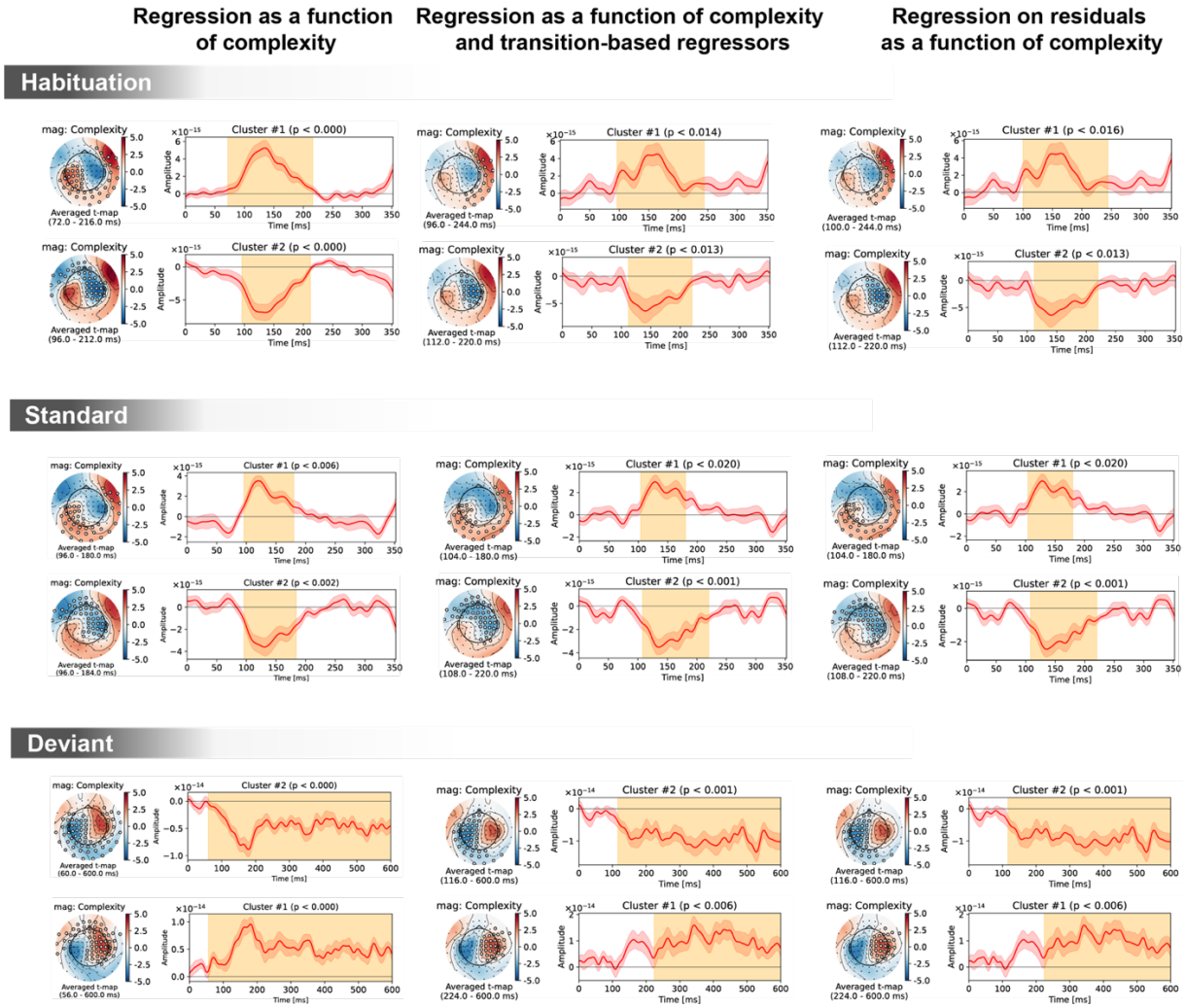

Figure S7. Spatiotemporal clusters for the complexity regressor in sensor space, shown separately for the 3 trial types (*Habituation, Standard, Deviant)* and 3 general linear models of MEG signals: with complexity alone (left column); with complexity, transition-based surprise and repeat/alternate (middle column); and with complexity after regressing out transition-based surprise and repeat/alternate signals. The clusters are very similar in all three cases, suggesting a robust effect of complexity irrespectively of transition statistics.

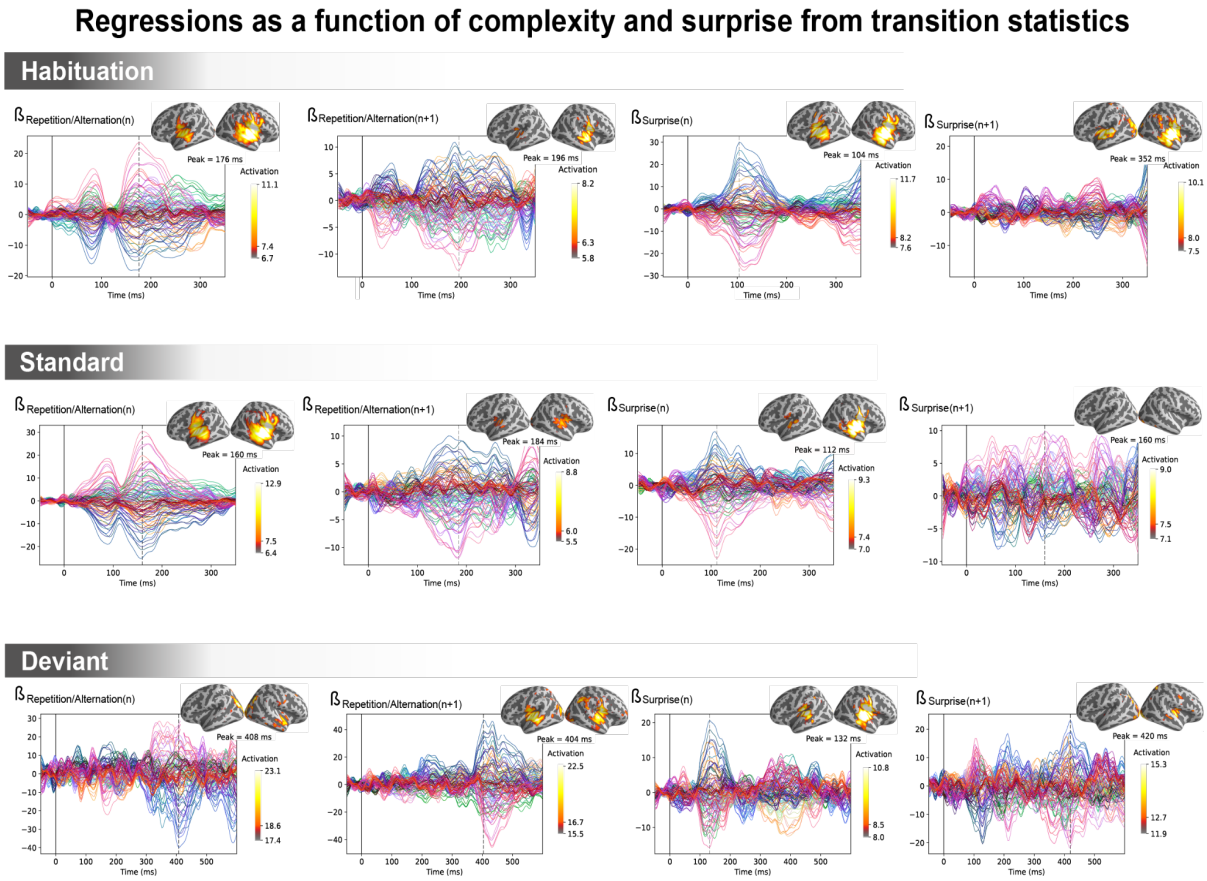

Figure S8. Amplitude of the regression coefficient ß for each MEG sensor for the 4 regressors of transition statistics: Repetition/Alternation for item *n* (presented at t=0 ms), Repetition/Alternation for item *n+1* (presented at t=250 ms), transition-based surprise for item *n* and transition-based surprise for item *n+1*. The transition-based surprise predictor is computed using an ideal observer estimating surprise over 100 past observations. The projection on the source space at the time of its maximal amplitude is also shown.

Table S1. fMRI complexity effect on standard trials (voxel-wise p < .001, uncorrected; cluster-wise p < .05, FDR corrected)

Positive LoT complexity effect in standard trials

Region	H	k	p(unc.)	p(FWE-corr)	T	x	y	z
Superior parietal gyrus, Precuneus	L/R	3254	<.0001	<.05	5.40	-12	-66	54
			<.0001	0.174	4.34	-24	-65	36
			<.0001	0.214	4.27	-26	-61	44
Lobule VI of cerebellar hemisphere	R	574	<.0001	<.05	5.09	27	-60	-26
Precentral gyrus, Superior frontal gyrus (dorsolateral)	L	1008	<.0001	<.05	4.88	-36	-4	54
			<.0001	0.177	4.34	-27	0	70
			<0.001	0.956	3.43	-15	2	63
Lobule VIII of cerebellar hemisphere	L	553	<.0001	0.147	4.39	-4	-79	-42
			<.0001	0.533	3.92	-12	-72	-48
			<.0001	0.581	3.88	-20	-65	-49

Negative LoT complexity effect in standard trials

Region	H	k	p(unc.)	p(FWE-corr)	T	x	y	z
Superior frontal gyrus (medial), Superior frontal gyrus (dorsolateral)	L/R	6072	<.0001	<.05	5.29	13	61	33
			<.0001	<.05	5.08	10	60	42
			<.0001	<.05	5.05	-26	60	28
IFG pars orbitalis, Lateral orbital gyrus, Posterior orbital gyrus	L	1093	<.0001	<.05	5.02	-50	28	-12
			<.0001	0.282	4.18	-38	42	-12
Putamen	L	713	<.0001	<.05	4.71	-27	-10	3
			<.0001	0.079	4.58	-29	-12	-9
			<0.001	0.860	3.60	-26	-2	-14
Inferior occipital gyrus, Middle occipital gyrus	L	561	<.0001	0.051	4.70	-26	-98	-9
Inferior temporal gyrus, Middle temporal gyrus	R	1035	<.0001	0.068	4.62	50	-7	-30
			<.0001	0.477	3.97	52	-23	-18
			<0.001	0.912	3.53	64	-19	-21
Angular gyrus, SupraMarginal gyrus	R	463	<.0001	0.084	4.56	64	-51	31
			<0.001	0.995	3.23	52	-63	44
Putamen	R	543	<.0001	0.094	4.53	30	-7	2
Middle cingulate & paracingulate gyri	L/R	1434	<.0001	0.129	4.43	6	-23	42
			<.0001	0.269	4.20	-4	-23	40
			<0.001	0.690	3.78	13	-49	36
Angular gyrus, Inferior parietal gyrus	L	1120	<.0001	0.171	4.35	-55	-58	31
			<.0001	0.466	3.98	-60	-51	42
Inferior temporal gyrus	L	614	<.0001	0.380	4.07	-54	-9	-37
			<0.001	0.844	3.62	-46	-19	-23
			<0.001	0.983	3.33	-54	-24	-18

Table S2. fMRI complexity effect on deviant trials (voxel-wise p < .001, uncorrected; cluster-wise p < .05, FDR corrected)

Positive LoT complexity effect in deviant trials

Region	H	k	p(unc.)	p(FWE-corr)	T	x	y	z
Superior frontal gyrus (medial)	L/R	474	<.0001	0.218	4.33	-1	60	38
			<0.001	0.773	3.77	-6	49	54
			<0.001	0.999	3.20	3	46	42

Negative LoT complexity effect in deviant trials

Region	H	k	p(unc.)	p(FWE-corr)	T	x	y	z
Superior and middle temporal, Precentral, Postcentral, SupraMarginal, Inferior parietal gyri, Insula, Rolandic operculum, Cerebellum (Lobule VI), Putamen	L/R	46888	<.0001	<.0001	7.58	-57	-21	26
			<.0001	<.0001	7.23	-36	0	5
			<.0001	<.0001	6.97	-48	-60	5
Middle cingulate & paracingulate gyri, Supplementary motor area	L/R	5241	<.0001	<.0001	7.12	-3	-5	54
			<.0001	<.0001	6.74	-6	11	37
			<.0001	<.05	4.87	-10	-26	44
Lobule VIII of cerebellar hemisphere	R	1242	<.0001	<0.001	5.94	18	-63	-51
			<.0001	0.508	4.01	17	-79	-53
Lobule VIII of cerebellar hemisphere	L	848	<.0001	0.051	4.75	-24	-58	-51
			<.0001	0.066	4.68	-17	-63	-55
			<0.001	0.999	3.19	-3	-63	-44
Calcarine fissure, Lingual gyrus	L/R	764	<.0001	0.137	4.47	11	-70	5
			<0.001	0.887	3.64	-13	-75	5
			<0.001	0.945	3.54	-20	-67	5

Positive LoT complexity effect in correctly-detected deviant trials

Region	H	k	p(unc.)	p(FWE-corr)	T	x	y	z
Superior frontal gyrus (medial)	L/R	1584	<.0001	<0.001	5.79	-1	37	44
			<.0001	0.225	4.30	-3	23	58
			<0.001	0.944	3.52	10	42	23

Negative LoT complexity effect in correctly-detected deviant trials

Region	H	k	p(unc.)	p(FWE-corr)	T	x	y	z
Superior temporal gyrus, Insula, Temporal pole	R	2359	<.0001	<.05	5.54	41	-5	-11
			<.0001	<.05	5.19	52	0	-7
			<.0001	0.397	4.10	62	-11	5
Superior temporal gyrus, Insula	L	1694	<.0001	<.05	5.02	-48	-4	-9
			<.0001	0.075	4.63	-33	-5	-4
			<.0001	0.206	4.33	-52	-5	9
Middle temporal gyrus, Superior temporal gyrus	R	1692	<.0001	<.05	4.76	60	-47	9
			<.0001	0.174	4.38	55	-30	3
			<.0001	0.234	4.29	57	-58	3
SupraMarginal gyrus, Middle temporal gyrus	L	1727	<.0001	0.110	4.52	-48	-54	-2
			<.0001	0.112	4.52	-54	-37	28
			<.0001	0.239	4.28	-59	-67	10
Supplementary motor area, Middle cingulate & paracingulate gyri	L/R	807	<.0001	0.127	4.48	1	-7	56
			<.0001	0.232	4.29	3	0	44